Contents

17 Compressible and Supersonic Flow **1**
17.1 Overview 1
17.2 Equations of Compressible Flow 3
17.3 Stationary, Irrotational, Quasi-One-Dimensional Flow 6
17.3.1 Basic Equations; Transition from Subsonic to Supersonic Flow 6
17.3.2 Setting up a Stationary, Transonic Flow 8
17.3.3 Rocket Engines 11
17.4 One Dimensional, Time-Dependent Flow 16
17.4.1 Riemann Invariants 16
17.4.2 Shock Tube 18
17.5 Shock Fronts 21
17.5.1 Junction Conditions Across a Shock; Rankine-Hugoniot Relations . . 21
17.5.2 Junction Conditions for Ideal Gas with Constant γ 28
17.5.3 Internal Structure of a Shock 29
17.5.4 Mach Cone 30
17.6 Self-Similar Solutions — Sedov-Taylor Blast Wave 31
17.6.1 The Sedov-Taylor Solution 31
17.6.2 Atomic Bomb 35
17.6.3 Supernovae 35

Chapter 17

Compressible and Supersonic Flow

Version 1217.2.K.tex 2 June 2013
Please send comments, suggestions, and errata via email to kip@caltech.edu or on paper to Kip Thorne, 350-17 Caltech, Pasadena CA 91125

Box 17.1
Reader's Guide

- This chapter relies heavily on Chap. 13 and on Secs. 16.2, 16.3 and 16.5 of Chap. 16.
- No subsequent chapters rely substantially on this one.

17.1 Overview

So far, we have mainly been concerned with flows that are slow enough that they may be treated as incompressible. We now consider flows in which the velocity approaches or even exceeds the speed of sound and in which changes of density along streamlines cannot be ignored. Such flows are common in aeronautics and astrophysics. For example, the motion of a rocket through the atmosphere is faster than the speed of sound in air. In other words, it is *supersonic*. Therefore, if we transform into the frame of the rocket, the flow of air past the rocket is also supersonic.

When the flow speed exceeds the speed of sound in some reference frame, it is not possible for a pressure pulse to travel upstream in that frame and change the direction of the flow. However, if there is a solid body in the way (e.g. a rocket or aircraft), the flow direction must change. In a supersonic flow, this change happens nearly discontinuously, through the formation of *shock fronts* at which the flow suddenly decelerates from supersonic to subsonic. An example is shown in Fig. 17.1. Shock fronts are an inevitable feature of supersonic flows.

In another example of supersonic flow, a rocket itself is propelled by the thrust created by its nozzle's escaping hot gases. These hot gases move through the rocket nozzle at

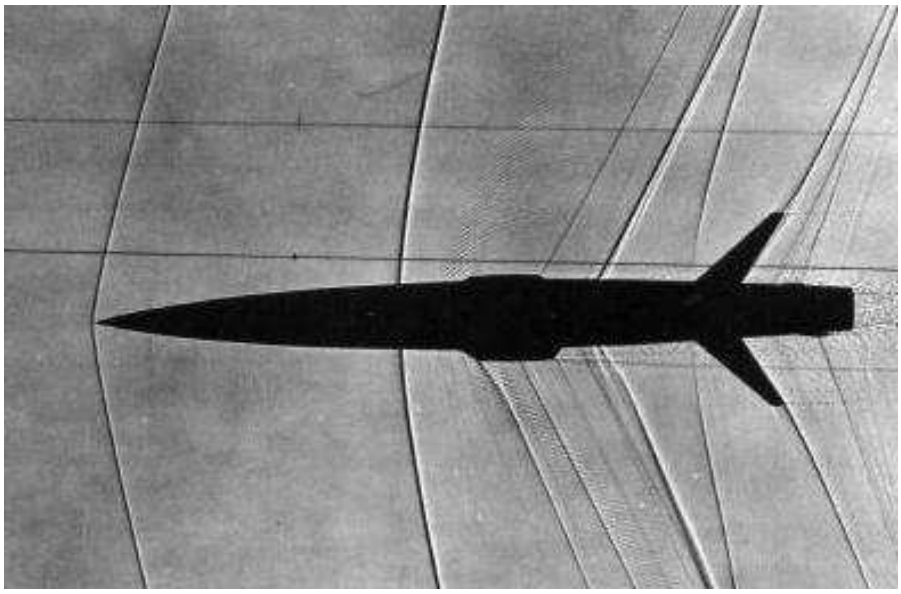

Fig. 17.1: Complex pattern of shock fronts formed around a model aircraft in a wind tunnel with air moving ten percent faster than the speed of sound (i.e. with Mach number $M = 1.1$.) Image from W. G. Vicenti; reproduced from Van Dyke 1982.

supersonic speeds, expanding and cooling as they accelerate. In this manner, the random thermal motion of the gas molecules is converted into an organized bulk motion that carries negative momentum away from the rocket and pushes it forward.

The solar wind furnishes yet another example of a supersonic flow. This high-speed flow of ionized gas is accelerated in the solar corona and removes a fraction $\sim 10^{-14}$ of the sun's mass every year. Its own pressure accelerates it to supersonic speeds of $\sim$ 400 km s^{-1}. When the outflowing solar wind encounters a planet, it is rapidly decelerated to subsonic speed by passing through a strong discontinuity, known as a *bow shock*, that surrounds the planet (Fig. 17.2). The bulk kinetic energy in the solar wind, built up during acceleration, is rapidly and irreversibly transformed into heat as it passes through this shock front.

In this chapter, we shall study some properties of supersonic flows. After restating the basic equations of compressible fluid dynamics (Sec. 17.2), we shall analyze three impor-

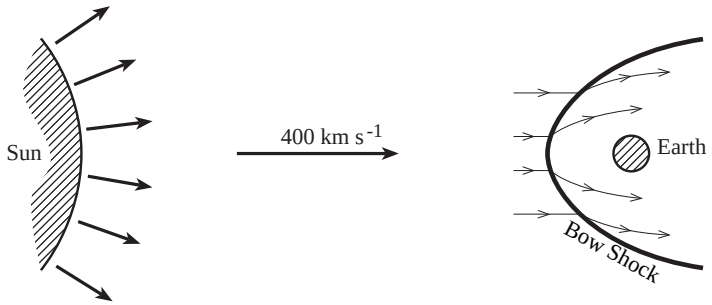

Fig. 17.2: The supersonic solar wind forms a type of shock front known as a bow shock when it passes by a planet.

tant, simple cases: stationary, quasi-one-dimensional flow (Sec. 17.3), time-dependent, one dimensional flow (Sec. 17.4), and normal adiabatic shock fronts (Sec. 17.5). In these sections, we shall apply the results of our analyses to some contemporary examples, including the Space Shuttle (Box 17.4), rocket engines, shock tubes, and the Mach cone, N-wave and sonic booms produced by supersonic projectiles and aircraft. In Sec. 17.6, we will develop similarity-solution techniques for supersonic flows and apply them to supernovae, underwater depth charges, and nuclear-bomb explosions in the earth's atmosphere.

As in our previous fluid-dynamics chapters, we strongly encourage readers to view relevant movies in parallel with reading this chapter. See Box 17.2.

Box 17.2
Movies Relevant to this Chapter

We strongly recommend that the reader view the following movies dealing with compressible and supersonic flows:

- *Effects of Fluid Compressibility* by Hunter Rouse (196?), available in 2013 at `http://www.iihr.uiowa.edu/research/publications-and-media/films-by-hunter-rouse/` . Covers most everything in this chapter except Riemann invariants. [KIP: CHECK]
- *Channel Flow of a Compressible Fluid* by Donald Coles (1968), film in the series by the National Committee for Fluid Mechanics Films, available in 2013 at `http://web.mit.edu/hml/ncfmf.html` . Focuses on shock fronts and quasi-one-dimensional flow through throats.
- *Waves in Fluids*, by A. E. Bryson (196?), film in the series by the National Committee for Fluid Mechanics Films, available in 2013 at `http://web.mit.edu/hml/ncfmf.html` . Includes segments on shock fronts and on hydraulic jumps.

17.2 Equations of Compressible Flow

In Chap. 13, we derived the equations of fluid dynamics, allowing for compressibility. We expressed them as laws of mass conservation [Eq. (13.29)], momentum conservation [$\partial(\rho\mathbf{v})/\partial t + \boldsymbol{\nabla}\cdot\mathbf{T} = 0$ with $\mathbf{T}$ as given in Table 13.3], and energy conservation [$\partial U/\partial t + \boldsymbol{\nabla}\cdot\mathbf{F} = 0$ with U and $\mathbf{F}$ as given in Table 13.3]; and also an evolution law for entropy [Eq. (13.76)]. When, as in this chapter, heat conduction is negligible ($\kappa \to 0$) and the gravitational field is a time-independent, external one (not generated by the flowing fluid), these equations become

$$\boxed{\frac{\partial\rho}{\partial t} + \nabla\cdot(\rho\mathbf{v}) = 0}\,, \tag{17.1a}$$

$$\boxed{\frac{\partial(\rho\mathbf{v})}{\partial t} + \nabla\cdot(P\mathbf{g} + \rho\mathbf{v}\otimes\mathbf{v} - 2\eta\boldsymbol{\sigma} - \zeta\theta\mathbf{g}) = \rho\boldsymbol{g}}\,, \tag{17.1b}$$

$$\boxed{\frac{\partial}{\partial t}\left[(\frac{1}{2}v^2+u+\Phi)\rho\right]+\boldsymbol{\nabla}\cdot[(\frac{1}{2}v^2+h+\Phi)\rho\mathbf{v}-2\eta\boldsymbol{\sigma}\cdot\mathbf{v}-\zeta\theta\mathbf{v}]=0}\,, \tag{17.1c}$$

$$\boxed{\frac{\partial(\rho s)}{\partial t}+\boldsymbol{\nabla}\cdot(\rho s\mathbf{v})=\frac{1}{T}\left(2\eta\boldsymbol{\sigma}:\boldsymbol{\sigma}+\zeta\theta^2\right)}\,. \tag{17.1d}$$

Here $\boldsymbol{\sigma}:\boldsymbol{\sigma}$ is index-free notation for $\sigma_{ij}\sigma_{ij}$.

Some comments are in order. Equation (17.1a) is the complete mass conservation equation (continuity equation) assuming that matter is neither added to nor removed from the flow. Equation (17.1b) expresses the conservation of momentum allowing for one external force, gravity. Other external forces (e.g. electromagnetic) can be added. Equation (17.1c), expressing energy conservation, includes a viscous contribution to the energy flux. If there are sources or sinks of fluid energy, then these must be included on the right-hand side of this equation. Possible sources of energy include chemical or nuclear reactions; possible energy sinks include cooling by emission of radiation. Equation (17.1d) expresses the evolution of entropy, and will also need modification if there are additional contributions to the energy equation. The right-hand side of this equation is the rate of increase of entropy due to viscous heating. This equation is not independent of the preceding equations and the laws of thermodynamics, but is often more convenient to use. In particular, one often uses it (together with the first law of thermodynamics) in place of energy conservation (17.1c).

These equations must be supplemented with an equation of state in the form $P(\rho,T)$ or $P(\rho,s)$. For simplicity, we shall often focus on an ideal gas (one with $P\propto\rho k_B T$) that undergoes adiabatic evolution with constant specific-heat ratio (adiabatic index; Ex. 5.4) γ, so the equation of state has the simple polytropic form (Box 13.2)

$$\boxed{P=K(s)\rho^\gamma}\,. \tag{17.2a}$$

Here $K(s)$ is a function of the entropy per unit mass s and is thus constant during adiabatic evolution, but will change across shocks because the entropy increases in a shock (Sec. 17.5). The value of γ depends on the number of thermalized internal degrees of freedom of the gas's constituent particles (Ex. 17.1). For a gas of free particles (e.g. fully ionized hydrogen), it is $\gamma=5/3$; for the earth's atmosphere, at temperatures between about 10 K and 400 K, it is $\gamma=7/5=1.4$ (Ex. 17.1).

For a polytropic gas with $P=K(s)\rho^\gamma$, we can integrate the first law of thermodynamics (Box 13.2) to obtain a formula for the internal energy per unit mass,

$$\boxed{u=\frac{P}{(\gamma-1)\rho}}\,, \tag{17.2b}$$

where we have assumed that the internal energy vanishes as the temperature $T\to 0$ and thence $P\to 0$. It will prove convenient to express the density ρ, the internal energy per unit mass u and the enthalpy per unit mass h in terms of the sound speed

$$\boxed{C=\sqrt{\left(\frac{\partial P}{\partial\rho}\right)_s}=\sqrt{\frac{\gamma P}{\rho}}} \tag{17.2c}$$

[Eq. (16.48)]. A little algebra gives

$$\boxed{\rho = \left(\frac{C^2}{\gamma K}\right)^{1/(\gamma-1)} \quad , \quad u = \frac{C^2}{\gamma(\gamma-1)} \; , \quad h = u + \frac{P}{\rho} = \frac{C^2}{\gamma - 1}} \; . \tag{17.2d}$$

****

EXERCISES

Exercise 17.1 ***Example: Values of γ*
Consider an ideal gas consisting of several different particle species, e.g. diatomic oxygen molecules and nitrogen molecules in the case of the Earth's atmosphere. Consider a sample of this gas with volume V, containing N_A particles of various species A, all in thermodynamic equilibrium at a temperature T sufficiently low that we can ignore effects of special relativity. Let species A have ν_A internal degrees of freedom with Hamiltonian quadratic in their generalized coordinates (e.g., rotation and vibration), that are sufficiently thermally excited to have reached energy equipartition. Then the equipartition theorem (Sec. 4.4.4) dictates that each such particle has $\frac{3}{2}k_BT$ of translational energy plus $\frac{1}{2}\nu_A k_B T$ of internal energy, and the fact that the gas is ideal dictates that each particle contributes k_BT/V to the pressure. Correspondingly, the sample's total energy E and pressure P are

$$E = \sum_A \left(\frac{3}{2} + \frac{\nu_A}{2}\right) N_A k_B T \; , \quad P = \frac{1}{V}\sum_A N_A k_B T \; . \tag{17.3a}$$

(a) Use the laws of thermodynamics to show that the specific heats at fixed volume and pressure are

$$C_V \equiv \left(\frac{T\partial S}{\partial T}\right)_{V,N_A} = \frac{E}{T} = \sum_A \left(\frac{3}{2} + \frac{\nu_A}{2}\right) N_A k_B \; , \quad C_P = \left(\frac{T\partial S}{\partial T}\right)_{P,N_A} = C_V + \frac{PV}{T} \; , \tag{17.3b}$$

so the ratio of specific heats is

$$\gamma = \frac{C_P}{C_V} = 1 + \frac{\sum_A N_A}{\sum_A N_A \left(\frac{3}{2} + \frac{\nu_A}{2}\right)} \; ; \tag{17.3c}$$

cf. Ex. 5.4.

(b) If there are no thermalized internal degrees of freedom, $\nu_A = 0$ (e.g., for a fully ionized, nonrelativistic gas), then $\gamma = 5/3$. For the earth's atmosphere, at temperatures between about 10 K and 400 K, the rotational degrees of freedom of the O_2 and N_2 molecules are thermally excited, but the temperature is too low to excite their vibrational degrees of freedom. Explain why this means that $\nu_{O_2} = \nu_{N_2} = 2$, which implies $\gamma = 7/5 = 1.4$. (Hint: there are just two orthogonal axes around which the diatomic molecule can rotate.)

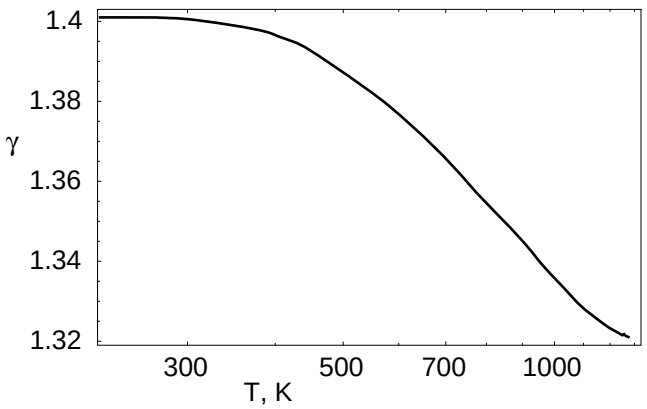

Fig. 17.3: The ratio of specific heats γ for air as a function of temperature.

(c) Between about 1300 K and roughly 10,000 K the vibrational degrees of freedom are thermalized but the molecules have not dissociated substantially into individual atoms nor become substantially ionized. Explain why this means that $\nu_{O_2} = \nu_{N_2} = 4$ in this temperature range, which implies $\gamma = 9/7 = 1.29$. (Hint: an oscillator has kinetic energy and potential energy.)

(d) At roughly 10,000 K the two oxygen atoms in O_2 dissociate from each other, the two nitrogen atoms in N_2 dissociate, and electrons begin to ionize from the atoms. Explain why this drives γ up toward $5/3 \simeq 1.67$.

The actual value of γ as a function of temperature for the range 200 K to 1300 K is shown in Fig. 17.3. Evidently, as stated above, $\gamma = 1.4$ is a good approximation only up to about 400 K, and the transition toward $\gamma = 1.29$ occurs gradually between about 400 K and 1400 K as the vibrational degrees of freedom gradually become thermalized and begin to obey the equipartion theorem (Sec. 4.4.4).

****

17.3 Stationary, Irrotational, Quasi-One-Dimensional Flow

17.3.1 Basic Equations; Transition from Subsonic to Supersonic Flow

In their full generality, the fluid dynamic equations (17.1) are quite unwieldy. To demonstrate some of the novel features of supersonic flow, we shall proceed as in earlier chapters: We shall specialize to a very simple type of flow in which the physical effects of interest are strong, and extraneous effects are negligible.

In particular, in this section, we shall seek insight into *smooth transitions between subsonic and supersonic flow* by restricting ourselves to a stationary ($\partial/\partial t = 0$), irrotational ($\boldsymbol{\nabla}\times\mathbf{v} = 0$) flow in which gravity and viscosity are negligible ($\Phi = \boldsymbol{g} = \eta = \zeta = 0$), as are various

effects not included in our general equations: chemical reactions, thermal conductivity and radiative losses. (We shall explore some effects of gravity in Ex. 17.4.) The vanishing viscosity implies [from the entropy evolution equation (17.1d)] that the entropy per baryon s is constant along each flow line. We shall assume that s is the same on all flow lines, so the flow is fully isentropic (s constant everywhere) and the pressure $P = P(\rho, s)$ can thus be regarded as a function only of the density, $P = P(\rho)$. When we need a specific form for $P(\rho)$, we will use the polytropic form $P = K(s)\rho^\gamma$ for an ideal gas with constant specific-heat ratio γ [Eqs. (17.2); Ex. 17.1], but much of our analysis will be done for a general isentropic $P(\rho)$. We will make one further approximation, that the flow is almost one dimensional. In other words, the velocity vectors all make small angles with each other in the region of interest.

These drastic simplifications are actually appropriate for many cases of practical interest. Granted these simplifications, we can consider a narrow bundle of streamlines which we call a *streamtube* and introduce, as a tool in studying it, its cross sectional area A normal to the flow (Fig. 17.4a).

As the flow is stationary, the equation of mass conservation (17.1a) states that the rate $\dot{m}$ at which mass passes through the streamtube's cross section must be independent of position along the tube:

$$\rho v A = \dot{m} = \text{constant}; \tag{17.4a}$$

here v is the speed of the fluid in the streamtube. Rewriting this in differential form, we obtain

$$\frac{dA}{A} + \frac{d\rho}{\rho} + \frac{dv}{v} = 0 \ . \tag{17.4b}$$

Because the flow is stationary and inviscid, the law of energy conservation (17.1c) reduces to Bernoulli's theorem [Eqs. (13.51), (13.50)]:

$$h + \frac{1}{2}v^2 = h_1 = \text{constant} \tag{17.4c}$$

along each streamline and thus along our narrow streamtube; here h_1 is the specific enthalpy at a location where the flow velocity v vanishes (e.g. in chamber 1 of Fig. 17.5a below).

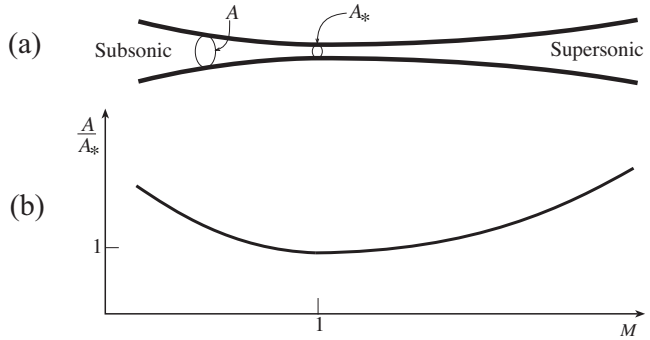

Fig. 17.4: Stationary, transonic flow in a converging then diverging streamtube. (a) The streamtube. (b) The flow's Mach number $M = v/C$ (horizontal axis) as a function of the streamtube's area A (vertical axis). The flow is subsonic to the left of the streamtube's throat $A = A_*$, sonic at the throat, and supersonic to the right.

Since the flow is adiabatic, we can use the first law of thermodynamics (Box 13.2) $dh = dP/\rho + Tds = dP/\rho = C^2 d\rho/\rho$ [where C is the speed of sound (17.2c)] to write Eq. (17.4c) in the differential form

$$\frac{d\rho}{\rho} + \frac{v dv}{C^2} = 0 \ . \tag{17.4d}$$

Finally and most importantly, we combine Eqs. (17.4b) and (17.4d) to obtain

$$\boxed{\frac{dv}{v} = \frac{dA/A}{M^2 - 1} \ , \qquad \frac{d\rho}{\rho} = \frac{dA/A}{M^{-2} - 1}} \ , \tag{17.5}$$

where

$$\boxed{M \equiv v/C} \tag{17.6}$$

is the *Mach number*. This Mach number is an important new dimensionless number that is used to characterize compressible flows. When the Mach number is less than 1, the flow is called *subsonic*; when $M > 1$, it is *supersonic*. By contrast with the Reynolds, Rossby and Ekman numbers, which are usually defined using a single set of (characteristic) values of the flow parameters (V, ν, Ω, L) and thus have a single value for any given flow, the Mach number by convention is defined at each point in the flow and thus is a flow variable $M(\mathbf{x})$ similar to $v(\mathbf{x})$ and $\rho(\mathbf{x})$.

Equations (17.5) make remarkable predictions, which we illustrate in Fig. 17.4 for a particular flow called "transonic"

1. The only locations along a streamtube at which M can be unity ($v = C$) are those where A is an extremum—e.g., for the streamtube of Fig. 17.4, the minimum $A = A_*$ (the tube's "throat").

2. At points along a streamtube where the flow is subsonic, $M < 1$ (left side of the streamtube in Fig. 17.4), v increases when A decreases, in accord with everyday experience.

3. At points where the flow is supersonic, $M > 1$ (right side of Fig. 17.4), v increases when A increases—just the opposite of everyday experience.

These conclusions are very useful in analyzing stationary, high-speed flows.

17.3.2 Setting up a Stationary, Transonic Flow

The reader may wonder, at this point, whether it is easy to set up a transonic flow in which the speed of the fluid changes continuously from subsonic to supersonic, as in Fig. 17.4 above. The answer is quite illuminating. We can illustrate the answer using two chambers maintained at different pressures, P_1 and P_2, and connected through a narrow channel, along which the cross sectional area passes smoothly through a minimum $A = A_*$, the channel's throat (Fig. 17.5a). When $P_2 = P_1$, there will be no flow between the two chambers. When we decrease P_2 slightly below P_1, there will be a slow subsonic flow through the channel (curves 1 in Fig. 17.5b,c). As we decrease P_2 further, there comes a point ($P = P_2^{\rm crit}$) at which the flow is forced to be transonic at the channel's throat $A = A_*$ (curves 2). For all

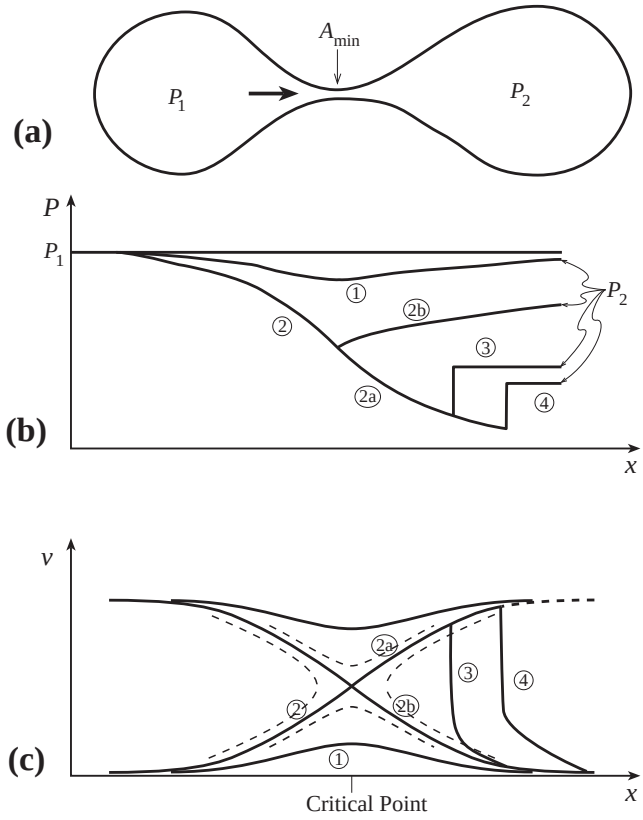

Fig. 17.5: Stationary flow through a channel between two chambers maintained at different pressures P_1 and P_2. When the pressure difference $P_1 - P_2$ is large enough, the flow is subsonic to the left of the channel's throat and supersonic to the right. As it nears or enters the second chamber, the supersonic flow must encounter a strong shock, where it decelerates abruptly to subsonic speed. The forms of the various velocity profiles $v(x)$ in drawing (c) are explained in Box 17.3.

pressures $P_2 < P_2^{\rm crit}$, the flow is also transonic at the throat and has a universal form to the left of and near the throat, independent of the value of P_2 (curves 2)—including a universal value $\dot{m}_{\rm crit}$ for the rate of mass flow through the throat! This universal flow is supersonic to the right of the throat (curves 2b), but it *must* be brought to rest in chamber 2, since there is a hard wall at the chamber's end. How is it brought to rest? Through a shock front, where it is driven subsonic almost discontinuously (curves 3 and 4; Sec. 17.5 below).

How, physically, is it possible for the transonic flow to have a universal form to the left of the shock? The key is that, in any supersonic region of the flow, disturbances are unable to propagate upstream, so the upstream fluid has no way of knowing what the pressure P_2 is in chamber 2. Although the flow to the left of the shock is universal, the location of the shock and the nature of the subsonic, post-shock flow *are* affected by P_2, since information can propagate upstream through that subsonic flow, from chamber 2 to the shock.

The reader might now begin to suspect that the throat, in the transonic case, is a very special location. It is, and that location is known as a *critical point* of the stationary flow. From a mathematical point of view, critical points are singular points of the equations (17.4) and (17.5) of stationary flow. This singularity shows up in the solutions to the equations, as

Box 17.3
Velocity Profiles for One-Dimensional Flow Between Chambers

Consider the adiabatic, stationary flow of an isentropic, polytropic fluid $P = K\rho^\gamma$ between the two chambers shown in Fig. 17.3. Describe the channel between chambers by its cross sectional area as a function of distance, $A(x)$, and describe the flow by the fluid's velocity $v(x)$ and its sound speed $C(x)$. There are two coupled algebraic equations for $v(x)$ and $C(x)$: mass conservation $\rho v A = \dot{m}$ [Eq. (17.4a)] and the Bernoulli theorem $h + \frac{1}{2}v^2 = h_1$ [Eq. (17.4c)], which, for our polytropic fluid, become [see Eqs. (17.2d)]:

$$C^{2/(\gamma-1)} v = (\gamma K)^{1/(\gamma-1)} \dot{m}/A \ , \quad \frac{C^2}{\gamma-1} + \frac{v^2}{2} = \frac{C_1^2}{\gamma-1} \ . \tag{1}$$

These equations are graphed in diagrams below for three different mass flow rates $\dot{m}$. Mass conservation [the first of Eqs. (1)] is a set of generalized hyperbolae, one for each value of the channel's area $A_* < A_a < A_b < A_c$. The Bernoulli theorem [the second of Eqs. (1)] is a single ellipse. On a chosen diagram (for a chosen $\dot{m}$), the dot at the intersection of the ellipse with a hyperbola tells us the flow velocity v and speed of sound C at each of the two points in the channel where the area A has the hyperbola's value.

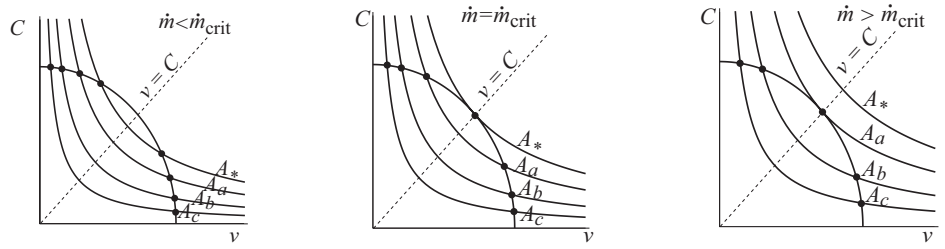

There is a critical mass flow rate $\dot{m}_{\rm crit}$ (central diagram), such that the hyperbola $A = A_*$ (the channel's throat) is tangent to the ellipse at the point $v = C$, so the flow is Mach 1 ($v = C$). For this $\dot{m}$, the sequence of dots along the ellipse, moving from lower right to upper left, represents the transonic flow, which begins subsonic and becomes supersonic (upward swooping solid curve in the drawing below); and the same sequence of dots, moving in the opposite direction from upper left to lower right, represents a flow that begins supersonic and smoothly transitions to subsonic (downward swooping solid curve, below). When $\dot{m} < \dot{m}_{\rm crit}$ (left diagram above; top and bottom quadrants below), the sequence of dots beginning at lower right reaches the throat $A = A_*$ at a subsonic velocity, so the solution climbs upward along the ellipse to that point then descends back down, mapping out a fully subsonic solution $v(x)$ below — and similarly for the dots on the upper branch of the ellipse, which map out a fully supersonic solution below. When $\dot{m} > \dot{M}_{\rm crit}$ (right diagram above), the dots map out curves in the left and right quadrants below that never reach the sonic point and are double valued for $v(x)$—and are thus unphysical. Therefore, the mass flow rate $\dot{m}$ can never exceed $\dot{m}_{\rm crit}$.

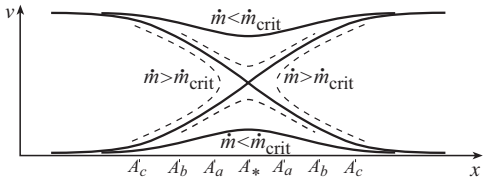

depicted in Fig. 17.5(c). The universal solution that passes transonically through the critical point (solution 2) joins onto two different solutions to the right of the throat: solution 2a, which is supersonic, and solution 2b, which is subsonic. Which solution occurs in practice depends on conditions downstream. Other solutions that are arbitrarily near this universal solution [dashed curves in Fig. 17.5(c)] are either double valued and consequently unphysical, or are everywhere subsonic or everywhere supersonic (in the absence of shocks); see Box 17.3 and Ex. 17.2.

The existence of critical points is a price we must pay, mathematically, for not allowing our equations to be time dependent. If we were to solve the time-dependent equations (which would then be partial differential equations), we would find that they change from elliptic to hyperbolic as the flow passes through a critical point.

From a physical point of view, critical points are the places where a sound wave propagating upstream remains at rest in the flow. They are therefore the one type of place from which time-dependent transients, associated with setting up the flow in the first place, cannot decay away (if the equations are dissipation-free, i.e., inviscid). Thus, even the time-dependent equations can display peculiar behaviors at a critical point. However, when dissipation is introduced, these peculiarities get smeared out.

****

EXERCISES

Exercise 17.2 *Problem: Explicit Solution for Flow Between Chambers When $\gamma = 3$*
For $\gamma = 3$ and for a channel with $A = A_*(1 + x^2)$, solve the flow equations (1) of Box 17.3 analytically and explicitly for $v(x)$, and verify that the solutions have the qualitative forms depicted in the bottom figure of Box 17.3.

****

17.3.3 Rocket Engines

We have shown that, in order to push a quasi-one-dimensional flow from subsonic to supersonic, one must send it through a throat. This result is exploited in the design of rocket engines and jet engines.

In a rocket engine, hot gas is produced by controlled burning of fuel in a large chamber, and the gas then escapes through a *converging-diverging* (also known as *De Laval*) nozzle, as shown in Fig. 17.6. The nozzle is designed with a skirt so the flow becomes supersonic smoothly when it passes through the nozzle's throat.

To analyze this flow in some detail, let us approximate it as precisely steady, isentropic and quasi-one-dimensional, and the gas as ideal and inviscid with constant ratio of specific heats γ. In this case, the enthalpy is $h = C^2/(\gamma - 1)$ [Eqs. (17.2d)], so Bernoulli's theorem (17.4c) reduces to

$$\frac{C^2}{(\gamma - 1)} + \frac{1}{2}v^2 = \frac{C_1^2}{(\gamma - 1)} \, . \tag{17.7}$$

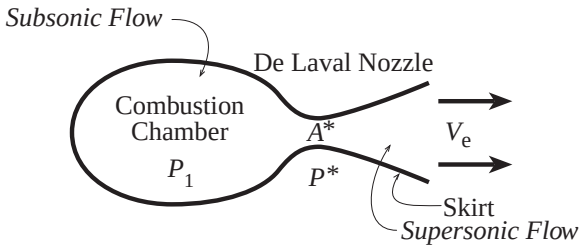

Fig. 17.6: Schematic illustration of a rocket engine. Note the skirt, which increases the thrust produced by the escaping exhaust gases.

Here C is the sound speed in the flow and C_1 is the "stagnation" sound speed, i.e., the sound speed evaluated in the rocket chamber where $v = 0$. Dividing this Bernoulli theorem by C^2 and manipulating, we learn how the sound speed varies with Mach number $M = v/C$:

$$C = C_1 \left[1 + \frac{\gamma - 1}{2} M^2\right]^{-1/2} . \tag{17.8}$$

From mass conservation [Eq. (17.4a)], we know that the cross sectional area A varies as $A \propto \rho^{-1} v^{-1} \propto \rho^{-1} M^{-1} C^{-1} \propto M^{-1} C^{(\gamma+1)/(1-\gamma)}$, where we have used $\rho \propto C^{2/(\gamma-1)}$ [Eqs. (17.2d)]. Combining with Eq. (17.8), and noting that $M = 1$ where $A = A_*$ (i.e., the flow is sonic at the throat), we find that

$$\frac{A}{A_*} = \frac{1}{M}\left[\frac{2}{\gamma+1} + \left(\frac{\gamma-1}{\gamma+1}\right) M^2\right]^{\frac{(\gamma+1)}{2(\gamma-1)}} , \tag{17.9}$$

The pressure P_* at the throat can be deduced from $P \propto \rho^\gamma \propto C^{2\gamma/(\gamma-1)}$ [Eqs. (17.2a) and (17.2d)] together with Eq. (17.8) with $M = 0$ and $P = P_1 =$ (stagnation pressure) in the chamber and $M = 1$ at the throat:

$$P_* = P_1 \left(\frac{2}{\gamma+1}\right)^{\frac{\gamma}{\gamma-1}} . \tag{17.10}$$

We use these formulas in Box 17.4 and Ex. 17.3 to evaluate, numerically, some features of the space shuttle and its rocket engines.

Bernoulli's theorem is a statement that the fluid's energy is conserved along a streamtube. (For conceptual simplicity we shall regard the entire interior of the nozzle as a single streamtube.) By contrast with energy, the fluid's momentum is not conserved, since it pushes against the nozzle wall as it flows. As the subsonic flow accelerates down the nozzle's converging region, the area of its streamtube diminishes, and the momentum flowing per second in the streamtube, $(P + \rho v^2)A$, decreases; momentum is being transferred to the nozzle wall. If the rocket did not have a skirt, but instead opened up completely to the outside world at its throat, the rocket thrust would be

$$T_* = (\rho_* v_*^2 + P_*)A_* = (\gamma + 1) P_* A_* . \tag{17.11}$$

This is much less than if momentum had been conserved along the subsonic, accelerating streamtubes.

Much of the "lost" momentum is regained, and the thrust is made significantly larger than T_*, by the force of the skirt on the stream tube in the diverging part of the nozzle (Fig. 17.6). The nozzle's skirt keeps the flow quasi-one-dimensional well beyond the throat, driving it more and more strongly supersonic. In this accelerating, supersonic flow the tube's rate of momentum flow $(\rho v^2 + P)A$ increases downstream, and there is a compensating increase of the rocket's forward thrust. This skirt-induced force accounts for a significant fraction of the thrust of a well-designed rocket engine.

Rockets work most efficiently when the exit pressure of the gas, as it leaves the base of the skirt, matches the external pressure in the surrounding air. When the pressure in the exhaust is larger than the external pressure, the flow is termed *under-expanded* and a pulse of low pressure, known as a *rarefaction* will be driven into the escaping gases causing them to expand and increasing their speed. However, the exhaust will now be pushing on the surrounding air, rather than on the rocket. More thrust could have been exerted on the rocket if the flow had not been under-expanded. By contrast, when the exhaust has a smaller pressure than the surrounding air (i.e., is *over-expanded*), shock fronts will form near the exit of the nozzle, affecting the fluid flow and sometimes causing separation of the flow from the nozzle's walls. It is important that the nozzle's skirt be shaped so that the exit flow is neither seriously over- nor under-expanded.

****

EXERCISES

Exercise 17.3 *Problem: Space Shuttle's Solid-Fuel Boosters*
Use the rough figures in Box 17.4 to estimate the energy released per unit mass in burning the fuel. Does your answer seem reasonable to you?

Exercise 17.4 ***Example: Adiabatic, Spherical Accretion of Gas Onto a Black Hole or Neutron Star*
Consider a black hole or neutron star with mass $\mathcal{M}$, at rest in interstellar gas that has constant ratio of specific heats γ. In this exercise you will derive some features of the adiabatic, spherical accretion of the gas onto the hole or star, a problem first solved by Bondi (1952). This exercise shows how gravity can play a role analogous to a De Laval nozzle: it can trigger a transition of the flow from subsonic to supersonic.

(a) Let ρ_∞ and C_∞ be the density and sound speed in the gas far from the hole (at radius $r = \infty$). Use dimensional analysis to estimate the rate of accretion of mass $\dot{\mathcal{M}}$ onto the star or hole, in terms of the parameters of the system: $\mathcal{M}$, γ, ρ_∞, C_∞, and Newton's gravitation constant G. [Hint: dimensional considerations alone cannot give the answer. Why? Augment your dimensional considerations by a knowledge of how the answer should scale with one of the parameters, e.g. the density, ρ_∞.]

(b) Give a simple physical argument, devoid of dimensional considerations, that produces the same answer for $\dot{\mathcal{M}}$, to within a multiplicative factor of order unity, as you deduced in part (a).

Box 17.4
Space Shuttle

NASA's (now defunct) Space Shuttle provides many nice examples of the behavior of supersonic flows. At launch, the shuttle and fuel had a mass $\sim 2\times10^6$ kg. The maximum thrust, $T \sim 3\times10^7$N, occurred at lift-off and gave the rocket an initial acceleration relative to the ground of $\sim 0.5g$. This increased to $\sim 3g$ as the fuel was burned and the total mass diminished. Most of the thrust was produced by two solid-fuel boosters that burned fuel at a combined rate of $\dot{m} \sim 10,000$ kg s^{-1} over a two minute period. Their combined thrust was $T \sim 2\times10^7$N averaged over the two minutes, from which we can estimate the speed of the escaping gases as they left the nozzles' skirts. Assuming this speed was quite supersonic (so $P_e \ll \rho_e v_e^2$), we estimate that $v_e \sim T/\dot{m} \sim 2$km s^{-1}. The combined exit areas of the two skirts was $A_e \sim 20$m^2, roughly four times the combined throat area, A_*. Using Eq. (17.9) with $\gamma \sim 1.29$, we deduce that the exit Mach number was $M_e \sim 3$.

From $T \sim \rho_e v_e^2 A_e$ and $P_e = \gamma C_e^2 \rho_e$ we deduce the exit pressure, $P_e \sim T/\gamma M_e^2 A_e \sim 8\times10^4$ N m^{-2}, about atmospheric. The stagnation pressure within the combustion region was [combine Eqs. (17.2a), (17.2d) and (17.8)]

$$P_1 \sim P_e\left[1+\frac{(\gamma-1)M_e^2}{2}\right]^{\frac{\gamma}{\gamma-1}} \sim 35 \text{ atmospheres.} \tag{1}$$

Of course, the actual operation was far more complex than this. For example, to optimize the final altitude, one must allow for the decreasing mass and atmospheric pressure as well as the two-dimensional gas flow through the nozzle.

The space shuttle can also be used to illustrate the properties of shock waves (Sec. 17.5 below). When the shuttle re-entered the atmosphere, it was highly supersonic, and therefore was preceded by a strong shock front that heated the onrushing air and consequently heated the shuttle. The shuttle continued moving supersonically down to 15 km altitude, and until this time it created a shock-front pattern that could be heard on the ground as a sonic boom. The maximum heating rate occurred at 70 km altitude. Here, the shuttle moved at $V \sim 7$ km s^{-1} and the sound speed is about 280 m s^{-1}, giving a Mach number of 25. For the specific heat ratio $\gamma \sim 1.5$ and mean molecular weight $\mu \sim 10$ appropriate to dissociated air, the strong-shock Rankine-Hugoniot relations (17.37), together with $P = (\rho/\mu m_p)k_B T$ and $C^2 = \gamma P/\rho$, predict the post-shock temperature

$$T \sim \frac{2(\gamma-1)\mu m_p V^2}{(\gamma+1)^2 k} \sim 9000\,\text{K} \tag{2}$$

Exposure to gas at this high temperature heated the shuttle's nose to ~ 1800 K.

There is a second, well-known consequence of this high temperature: it is sufficient to ionize the air partially as well as dissociate it. As a result, during reentry the shuttle was surrounded by a sheath of plasma, which, as we shall discover in Chap. 19, prevented radio communication. The blackout lasted for about 12 minutes.

(c) Because the neutron star and black hole are both very compact with intense gravity near their surfaces, the inflowing gas is guaranteed to accelerate to supersonic speeds as it falls in. Explain why the speed will remain supersonic in the case of the hole, but must transition through a shock to subsonic flow near the surface of the neutron star. If the star has the same mass $\mathcal{M}$ as the hole, will the details of its accretion flow $[\rho(r),\, C(r),\, v(r)]$ be the same as or different from those for the hole, outside the star's shock? Will the mass accretion rates $\dot{\mathcal{M}}$ be the same or different? Justify your answers, physically.

(d) By combining the Euler equation for $v(r)$ with the equation of mass conservation, $\dot{\mathcal{M}} = 4\pi r^2 \rho v$, and with the sound-speed equation $C^2 = (\partial P/\partial\rho)_s$, show that

$$(v^2 - C^2)\frac{1}{\rho}\frac{d\rho}{dr} = \frac{G\mathcal{M}}{r^2} - \frac{2v^2}{r}\ . \tag{17.12}$$

Thereby deduce that the flow speed v_s, sound speed C_s, and radius r_s at the *sonic point* (the radius of transition from subsonic to supersonic flow) are related by

$$v_s^2 = C_s^2 = \frac{G\mathcal{M}}{2r_s}\ . \tag{17.13}$$

(e) By combining with the Bernoulli equation (with the effects of gravity included), deduce that the sound speed at the sonic point is related to that at infinity by

$$C_s^2 = \frac{2C_\infty^2}{5 - 3\gamma} \tag{17.14}$$

and that the radius of the sonic point is

$$r_s = \frac{(5-3\gamma)}{4}\frac{G\mathcal{M}}{C_\infty^2}\ . \tag{17.15}$$

Thence also deduce a precise value for the mass accretion rate $\dot{\mathcal{M}}$ in terms of the parameters of the problem. Compare with your estimate of $\dot{\mathcal{M}}$ in parts (a) and (b). [Comment: For $\gamma = 5/3$, which is the value for hot, ionized gas, this analysis places the sonic point at an arbitrarily small radius. In this limiting case (i) general relativistic effects strengthen the gravitational field, thereby moving the sonic point well outside the star or hole, and (ii) your answer for $\dot{\mathcal{M}}$ has a finite value close to the general relativistic prediction. See Ex. 26.10.

(f) Much of the interstellar medium is hot and ionized, with density about one proton per cubic centimeter and temperature about 10^4 K. In such a medium, what is the mass accretion rate onto a 10 solar mass hole, and approximately how long does it take for the hole's mass to double?

****

17.4 One Dimensional, Time-Dependent Flow

17.4.1 Riemann Invariants

Let us turn now to time-dependent flows. Again we confine our attention to the simplest situation that illustrates the physics, in this case, truly one-dimensional motion of an isentropic fluid in the absence of viscosity, thermal conductivity and gravity, so the flow is adiabatic as well as isentropic (entropy constant in time as well as space). The motion of the gas in such a flow is described by the equation of continuity (17.1a) and the Euler equation (17.1b) specialized to one dimension:

$$\frac{d\rho}{dt} = -\rho\frac{\partial v}{\partial x} \ , \qquad \frac{dv}{dt} = -\frac{1}{\rho}\frac{\partial P}{\partial x} \ , \tag{17.16}$$

where

$$\frac{d}{dt} = \frac{\partial}{\partial t} + v\frac{\partial}{\partial x} \tag{17.17}$$

is the convective (advective) time derivative—the time derivative moving with the fluid.

Given an isentropic equation of state $P = P(\rho)$ that relates the pressure to the density, these two nonlinear equations can be combined into a single second order differential equation in the velocity. However, it is more illuminating to work with the first-order set. As the gas is isentropic, the density ρ and sound speed $C = (dP/d\rho)^{1/2}$ can both be regarded as functions of a single thermodynamic variable, which we choose to be the pressure.

Taking linear combinations of Eqs. (17.16), we obtain two partial differential equations

$$\frac{\partial v}{\partial t} \pm \frac{1}{\rho C}\frac{\partial P}{\partial t} + (v \pm C)\left(\frac{\partial v}{\partial x} \pm \frac{1}{\rho C}\frac{\partial P}{\partial x}\right) = 0 \ , \tag{17.18}$$

which together are equivalent to Eqs. (17.16). We can rewrite these equations in terms of *Riemann invariants*

$$\boxed{J_\pm \equiv v \pm \int \frac{dP}{\rho C}} \tag{17.19}$$

and *characteristic speeds*

$$\boxed{V_\pm \equiv v \pm C} \tag{17.20}$$

in the following way:

$$\boxed{\left(\frac{\partial}{\partial t} + V_\pm\frac{\partial}{\partial x}\right) J_\pm = 0} \ . \tag{17.21}$$

Equation (17.21) tells us that the convective derivative of each Riemann invariant $J_\pm$ vanishes for an observer who moves, not with the fluid speed, but, instead, with the speed $V_\pm$. We say that each Riemann invariant is conserved along its characteristic (denoted by $\mathcal{C}_\pm$), which is a path through spacetime satisfying

$$\boxed{\mathcal{C}_\pm : \quad \frac{dx}{dt} = v \pm C} \ . \tag{17.22}$$

Note that in these equations, both v and C are functions of x and t.

The characteristics have a natural interpretation. They describe the motion of small disturbances traveling backward and forward relative to the fluid at the local sound speed. As seen in the fluid's local rest frame $v = 0$, two neighboring events in the flow, separated by a small time interval Δt and a space interval $\Delta x = +C\Delta t$ so that they lie on the same $\mathcal{C}_+$ characteristic, will have small velocity and pressure differences satisfying $\Delta v = -\Delta P/\rho C$ [as one can deduce from Eqs. (17.16) with $v = 0$, $d/dt = \partial/\partial t$ and $C^2 = dP/d\rho$]. Now, for a linear sound wave, propagating along the positive x direction, Δv and ΔP will separately vanish. However in a nonlinear wave, only the combination $\Delta J_+ = \Delta v + \Delta P/\rho C$ will vanish along $\mathcal{C}_+$. Integrating over a finite interval of time, we recover the constancy of J_+ along the characteristic $\mathcal{C}_+$ [Eq. (17.21)].

The Riemann invariants provide a general method for deriving the details of the flow from initial conditions. Suppose that the fluid velocity and the thermodynamic variables are specified over an interval of x, designated ∂S, at an initial time $t = 0$ (Fig. 17.7). This means that $J_\pm$ are also specified over this interval. We can then determine $J_\pm$ at any point $\mathcal{P}$ in the *domain of dependence* S of ∂S (i.e., at any point linked to ∂S by two characteristics $\mathcal{C}_\pm$) by simply propagating each of $J_\pm$ unchanged along its characteristic. From these values of $J_\pm$ at $\mathcal{P}$, we can solve algebraically for all the other flow variables (v, P, ρ, ...) at $\mathcal{P}$. To learn the evolution outside the domain of dependence S, we must specify the initial conditions outside ∂S.

In practice, we do not actually know the characteristics $\mathcal{C}_\pm$ until we have solved for the flow variables, so we must solve for the characteristics as part of the solution process. This means, in practice, that the solution involves algebraic manipulations of (i) the equation of state and the relations $J_\pm = v \pm \int dP/\rho C$, which give $J_\pm$ in terms of v and C; and

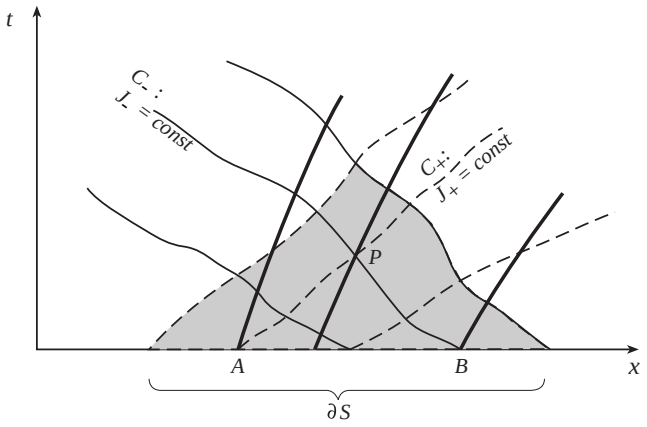

Fig. 17.7: Spacetime diagram showing the characteristics (thin solid and dashed lines) for a one dimensional adiabatic flow of an isentropic gas. The paths of the fluid elements are shown as thick solid lines. Initial data are presumed to be specified over some interval ∂S of x at time $t = 0$. The Riemann invariant J_+ is constant along each characteristic $\mathcal{C}_+$ (thin dashed line) and thus at point $\mathcal{P}$ it has the same value, unchanged, as at point $\mathcal{A}$ in the initial data. Similarly J_- is invariant along each characteristic $\mathcal{C}_-$ (thin solid line) and thus at $\mathcal{P}$ it has the same value as at $\mathcal{B}$. The shaded area of spacetime is the domain of dependence S of ∂S.

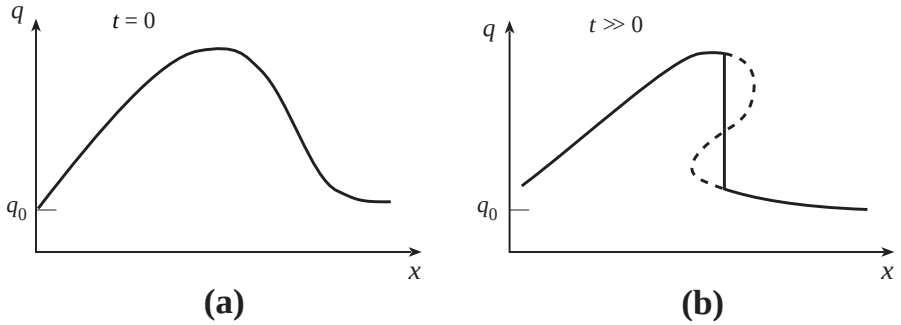

Fig. 17.8: Evolution of a nonlinear sound wave. The fluid at the crest of the wave moves faster than the fluid in the trough. Mathematically, the flow eventually becomes triple-valued (dashed curve). Physically, a shock wave develops (vertical solid line).

(ii) the conservation laws that $J_\pm$ are constant along $\mathcal{C}_\pm$, i.e. along curves $dx/dt = v \pm C$. These algebraic manipulations have the goal of deducing $C(x,t)$ and $v(x,t)$ from the initial conditions on ∂S. We shall exhibit a specific example in the next subsection.

We can use Riemann invariants to understand qualitatively how a nonlinear sound wave evolves with time. If the wave propagates in the positive x direction into previously undisturbed fluid (fluid with $v = 0$), then the J_- invariant, propagating backward along $\mathcal{C}_-$, is constant everywhere, so $v = \int dP/\rho C + \text{constant}$. Let us use $q \equiv \int dP/\rho C$ as our wave variable. For an ideal gas with constant ratio of specific heats γ, $q = 2C/(\gamma - 1)$, so our oscillating wave variable is essentially the oscillating sound speed. Constancy of J_- then says that $v = q - q_0$, where q_0 is the stagnation value of q, i.e. the value of q in the undisturbed fluid in front of the wave.

Now, $J_+ = v + q$ is conserved on each rightward characteristic $\mathcal{C}_+$, and so both v and q are separately conserved on each $\mathcal{C}_+$. If we sketch a profile of the wave pulse as in Fig. 17.8 and measure its amplitude using the quantity q, then the relation $v = q - q_0$ says that the fluid at the crest of the wave moves faster than the fluid in a trough. This causes the leading edge of the wave to steepen, a process we have already encountered in our discussion of shallow-water solitons (Fig. 16.4). Now, sound waves, by contrast with shallow-water waves (where dispersion counteracts the steepening), are non-dispersive so the steepening will continue until $|dv/dx| \to \infty$ (Fig. 17.8). When the velocity gradient becomes sufficiently large, viscosity and dissipation will become strong, producing an increase of entropy and a breakdown of our isentropic flow. This breakdown and entropy increase will occur in an extremely thin region—a shock wave, which we shall study in Sec. 17.5.

17.4.2 Shock Tube

We have shown how one dimensional isentropic flows can be completely analyzed by propagating the Riemann invariants along characteristics. Let us illustrate this in more detail by analyzing a shock tube, a laboratory device for creating supersonic flows and studying the behavior of shock waves. In a shock tube, high pressure gas is retained at rest in the left half of a long tube by a thin membrane (Fig. 17.9a). At time $t = 0$, the membrane is ruptured by a laser beam and the gas rushes into the tube's right half, which has usually been evacuated.

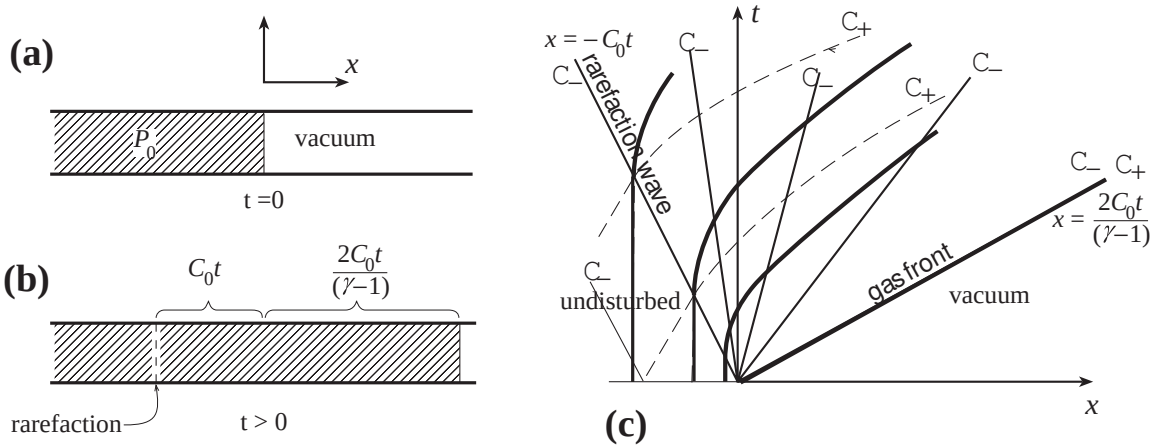

Fig. 17.9: Shock Tube. (a) At $t \leq 0$ gas is held at rest at high pressure P_0 in the left half of the tube. (b) At $t > 0$ the high-pressure gas moves rightward down the tube at high speed, and a rarefaction wave propagates leftward at the sound speed. (c) Space-time diagram showing the flow's characteristics ($\mathcal{C}_+$: thin dashed lines; $\mathcal{C}_-$: thin solid lines) and fluid paths (thick solid lines). To the left of the rarefaction wave, $x < -C_o t$, the fluid is undisturbed. To the right of the gas front, $x > [2/(\gamma-1)]C_o t$, is undisturbed (near) vacuum

Diagnostic photographs and velocity and pressure measurements are synchronized with the onset of the flow.

Let us idealize the operation of a shock tube by assuming, once more, that the gas is ideal with constant γ, so that $P \propto \rho^\gamma$. For times $t \leq 0$, we suppose that the gas has uniform density ρ_0 and pressure P_0 (and consequently uniform sound speed C_0) at $x \leq 0$, and that $\rho = P = 0$ at $x \geq 0$. At time $t = 0$, the barrier is removed and the gas flows towards positive x. Now, the first Riemann invariant J_+ is conserved on $\mathcal{C}_+$, which originates in the static gas, so it has the value

$$J_+ = v + \frac{2C}{\gamma - 1} = \frac{2C_0}{\gamma - 1} \ . \tag{17.23}$$

Note that in this case, the invariant is the same on all rightward characteristics, i.e. throughout the flow, so

$$v = \frac{2(C_0 - C)}{\gamma - 1} \quad \text{everywhere.} \tag{17.24}$$

The second invariant is

$$J_- = v - \frac{2C}{\gamma - 1} \ . \tag{17.25}$$

Its constant values are not so easy to identify because those characteristics $\mathcal{C}_-$ that travel through the perturbed flow all emerge from the origin, where v and C are indeterminate; cf. Fig. 17.9c. However, by combining Eq. (17.24) with Eq. (17.25), we deduce that v and C are separately constant on each characteristic $\mathcal{C}_-$. This enables us, trivially, to solve the differential equation $dx/dt = v - C$ for the leftward characteristics $\mathcal{C}_-$, obtaining

$$\mathcal{C}_- : \quad x = (v - C)t \ . \tag{17.26}$$

Here we have set the constant of integration equal to zero so as to obtain all the characteristics that propagate through the perturbed fluid. (For those in the unperturbed fluid, $v = 0$ and $C = C_0$, so $x = x_0 - C_0 t$ with $x_0 < 0$ the characteristic's initial location.)

Now Eq. (17.26) is true on each characteristic in the perturbed fluid. Therefore it is true throughout the perturbed fluid. We can therefore combine Eqs. (17.24), (17.26) to solve for $v(x,t)$ and $C(x,t)$ throughout the perturbed fluid. That solution, together with the obvious solution (same as initial data) to the left and right of the perturbed fluid, is:

$$\begin{aligned} &v = 0\ , \quad C = C_0 \quad \text{at } x < -C_0 t\ , \\ &v = \frac{2}{\gamma+1}\left(C_0 + \frac{x}{t}\right)\ , \quad C = \frac{2C_0}{\gamma+1} - \left(\frac{\gamma-1}{\gamma+1}\right)\frac{x}{t} \quad \text{at } -C_0 t < x < \frac{2C_0}{\gamma-1}t\ , \\ &\text{vacuum prevails at } x > \frac{2C_0}{\gamma-1}t\ . \end{aligned} \tag{17.27}$$

Notice, in this solution, that the gas at $x < 0$ remains at rest until a *rarefaction wave* from the origin reaches it. Thereafter it is accelerated rightward by the local pressure gradient, and as it accelerates it expands and cools so its speed of sound C goes down; asymptotically it reaches zero temperature as exhibited by $C = 0$ and an asymptotic speed $v = 2C_0/(\gamma-1)$ [cf. Eq. (17.23)]; see Fig. 17.9b,c. In the expansion, the internal random velocity of the gas molecules is transformed into an ordered velocity just as in a rocket's exhaust. However, the total energy per unit mass in the stationary gas is $u = C_0^2/\gamma(\gamma-1)$ [Eq. (17.2d)], which is less than the asymptotic kinetic energy per unit mass of $2C_0^2/(\gamma-1)^2$. The missing energy has gone into performing work on the gas that is still struggling to reach its asymptotic speed.

In the more realistic case, where there initially is some low-density gas in the evacuated half of the tube, the expanding driver gas creates a strong shock as it plows into the low-density gas; hence the name "shock tube". In the next section we shall explore the structure of this and other shock fronts.

****

EXERCISES

Exercise 17.5 *Problem: Fluid Paths in Free Expansion*
We have computed the velocity field for a freely expanding gas in one dimension, Eq. (17.27). Use this result to show that the path of an individual fluid element, which begins at $x = x_0 < 0$, is

$$x = \frac{2C_0 t}{\gamma-1} + \left(\frac{\gamma+1}{\gamma-1}\right) x_0 \left(\frac{-C_0 t}{x_0}\right)^{\frac{2}{\gamma+1}} \quad \text{at } 0 < -\frac{x_0}{C_0} < t\ .$$

Exercise 17.6 *Problem: Riemann Invariants for Shallow-Water Flow; Breaking of a Dam*
Consider the one-dimensional flow of shallow water in a straight, narrow channel, neglecting dispersion and boundary layers. The equations governing the flow, as derived and discussed in Box 16.3 and Eqs. 16.23, are

$$\frac{\partial h}{\partial t} + \frac{\partial (hv)}{\partial x} = 0\ , \quad \frac{\partial v}{\partial t} + v\frac{\partial v}{\partial x} + g\frac{\partial h}{\partial x} = 0\ . \tag{17.28}$$

Here $h(x,t)$ is the height of the water and $v(x,t)$ is its depth-independent velocity.

(a) Find two Riemann invariants $J_\pm$ for these equations, and find two conservation laws for these $J_\pm$ which are equivalent to the shallow-water equations (17.28).

(b) Use these Riemann invariants to demonstrate that shallow-water waves steepen in the manner depicted in Fig. 16.4, a manner analogous to the peaking of the nonlinear sound wave in Fig. 17.8.

(c) Use these Riemann invariants to solve for the flow of water $h(x,t)$ and $v(x,t)$ after a dam breaks (the problem posed in Ex. 16.9, and there solved via similarity methods). The initial conditions, at $t = 0$, are $v = 0$ everywhere, and $h = h_o$ at $x < 0$, $h = 0$ (no water) at $x > 0$.

****

17.5 Shock Fronts

We have just demonstrated that in an ideal gas with constant adiabatic index γ, large perturbations to fluid dynamical variables inevitably evolve to form a divergently large velocity gradient—a *shock front* or a *shock wave* or simply a *shock*. Now, when the velocity gradient becomes large, we can no longer ignore the viscous stress because the viscous terms in the Navier-Stokes equation involve second derivatives in space, whereas the inertial term involves only first derivatives. As in turbulence and in boundary layers, so also in a shock front, the viscous stresses convert the fluid's ordered, bulk kinetic energy into microscopic kinetic energy, i.e. thermal energy. The ordered fluid velocity $\mathbf{v}$ thereby is rapidly—almost discontinuously—reduced from supersonic to subsonic, and the fluid is heated.

The cooler, supersonic region of incoming fluid is said to be *ahead of* or *upstream from* the shock, and it hits the shock's *front side*; the hotter, subsonic region of outgoing fluid is said to be *behind* or *downstream from* the shock, and it emerges from the shock's *back side*; see Fig. 17.10 below.

17.5.1 Junction Conditions Across a Shock; Rankine-Hugoniot Relations

Viscosity is crucial to the internal structure of the shock, but it is just as negligible in the downstream flow behind the shock as in the upstream flow ahead of the shock, since there velocity gradients are modest again. Remarkably, if (as is usually the case) the shock front is very thin compared to the length scales in the upstream and downstream flows, and the time for the fluid to pass through the shock is short compared to the upstream and downstream timescales, then we can deduce the net influence of the shock on the flow without any reference to the viscous processes that operate within the shock, and without reference to the shock's detailed internal structure. We do so by treating the shock as a discontinuity

across which certain junction conditions must be satisfied. This is similar to electromagnetic theory, where the junction conditions for the electric and magnetic fields across a material interface are independent of the detailed structure of the interface.

The keys to the shock's junction conditions are the conservation laws for mass, momentum and energy: The fluxes of mass, momentum, and energy must usually be the same in the downstream flow, emerging from the shock, as in the upstream flow, entering the shock. To understand this, we first note that, because the time to pass through the shock is so short, mass, momentum and energy cannot accumulate in the shock, so the flow can be regarded as stationary. In a stationary flow, the mass flux is always constant, as there is no way to create new mass or destroy old mass. Its continuity across the shock can be written as

$$\boxed{[\rho \mathbf{v} \cdot \mathbf{n}] = 0}\,, \tag{17.29a}$$

where $\mathbf{n}$ is the unit normal to the shock front and the square bracket means the difference in the values on the downstream and upstream sides of the shock. Similarly, the total momentum flux, $\mathbf{T} \cdot \mathbf{n}$, must be conserved in the absence of external forces. Now $\mathbf{T}$ has both a mechanical component, $P\mathbf{g} + \rho \mathbf{v} \otimes \mathbf{v}$ and a viscous component, $-\zeta\theta\mathbf{g} - 2\eta\boldsymbol{\sigma}$. However, the viscous component is negligible in the upstream and downstream flows, which are being matched to each other, so the mechanical component by itself must be conserved across the shock front:

$$\boxed{[(P\mathbf{g} + \rho \mathbf{v} \otimes \mathbf{v}) \cdot \mathbf{n}] = 0}\,. \tag{17.29b}$$

Similar remarks apply to the energy flux, though here we must be slightly more restrictive. There are three ways that a change in the energy flux could occur. First, energy may be added to the flow by chemical or nuclear reactions that occur in the shock front. Second, the gas may be heated to such a high temperature that it will lose energy in the shock front through the emission of radiation. Third, energy may be conducted far upstream by suprathermal particles so as to pre-heat the incoming gas. This will thicken the shock front and may make it so thick that it can no longer sensibly be approximated as a discontinuity. If any of these processes are occurring, we must check to see whether they are strong enough to significantly influence energy conservation across the shock. What such a check often reveals is that preheating is negligible, and the lengthscales over which the chemical and nuclear reactions and radiation emission operate are much greater than the length over which viscosity acts. In this case we can conserve energy flux across the viscous shock and then follow the evolutionary effects of reactions and radiation (if significant) in the downstream flow.

A shock with negligible preheating, and with negligible radiation emission and chemical and nuclear reactions inside the shock, will have the same energy flux in the departing, downstream flow as in the entering, upstream flow, i.e., they will satisfy

$$\boxed{\left[\left(\frac{1}{2}v^2 + h\right)\rho \mathbf{v} \cdot \mathbf{n}\right] = 0}\,. \tag{17.29c}$$

Shocks which satisfy the conservation laws of mass, momentum and energy, Eqs. (17.29), are said to be *adiabatic*.

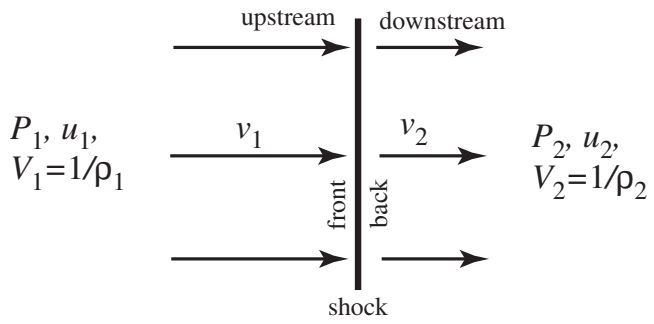

Fig. 17.10: Terminology and notation for a shock front and the flow into and out of it.

By contrast, with mass, momentum and energy, the entropy will not be conserved across a shock front, since viscosity and other dissipative processes increase the entropy as the fluid flows through the shock. So far, the only type of dissipation which we have discussed is viscosity and this is sufficient by itself to produce a shock front and keep it thin. However, heat conduction (Sec. 18.2) and electrical resistivity, which is important in magnetic shocks (Chap. 19), can also contribute to the dissipation and can influence the detailed structure of the shock front.

For an adiabatic shock, the three requirements of mass, momentum and energy conservation [Eqs. (17.29)], known collectively as the *Rankine-Hugoniot relations*, enable us to relate the downstream flow and its thermodynamic variables to their upstream counterparts.[1]

Let us work in a reference frame where the incoming flow is normal to the shock front and the shock is at rest, so the flow is stationary in the shock's vicinity. Then the conservation of tangential momentum — the tangential component of Eq. (17.29b) — tells us that the outgoing flow is also normal to the shock in our chosen reference frame. We say that the shock is *normal*, not *oblique*.

We use the subscripts 1, 2 to denote quantities measured ahead of and behind the shock respectively; i.e., 1 is the incoming flow and 2 is the outgoing flow (Fig. 17.10). The Rankine-Hugoniot relations (17.29) then take the forms

$$\rho_2 v_2 = \rho_1 v_1 = j \ , \tag{17.30a}$$

$$P_2 + \rho_2 v_2^2 = P_1 + \rho_1 v_1^2 \ , \tag{17.30b}$$

$$h_2 + \frac{1}{2} v_2^2 = h_1 + \frac{1}{2} v_1^2 \ , \tag{17.30c}$$

where j is the mass flux, which is determined by the upstream flow.

These equations can be brought into a more useful form by replacing the density ρ with the *specific volume* $V \equiv 1/\rho$, replacing the specific enthalpy h by its value in terms of P and

[1] The existence of shocks was actually understood quite early on, more or less in this way, by Stokes. However, he was persuaded by his former student Rayleigh and others that such discontinuities were impossible because they would violate energy conservation. With a deference that professors traditionally show their students, Stokes believed him. They were both making an error in their analysis of energy conservation, due to inadequate understanding of thermodynamics in that era.

V, $h = u + P/\rho = u + PV$, and performing some algebra; the result is

$$\boxed{u_2 - u_1 = \frac{1}{2}(P_1 + P_2)(V_1 - V_2)}\,, \tag{17.31a}$$

$$\boxed{j^2 = \frac{P_2 - P_1}{V_1 - V_2}}\,, \tag{17.31b}$$

$$\boxed{v_1 - v_2 = [(P_2 - P_1)(V_1 - V_2)]^{1/2}}\,. \tag{17.31c}$$

This is the most widely used form of the Rankine-Hugoniot relations. It must be augmented by an equation of state in the form

$$\boxed{u = u(P, V)}\,. \tag{17.32}$$

Some of the physical content of these Rankine-Hugoniot relations is depicted in Fig. 17.11. The thermodynamic state of the upstream (incoming) fluid is the point (V_1, P_1) in this volume-pressure diagram. The thick solid curve, called the *shock adiabat*, is the set of all possible downstream (outgoing) fluid states. This shock adiabat can be computed by combining Eq. (17.31a) with the equation of state (17.32). Those equations will actually give a curve that extends away from (V_1, P_1) in both directions, up-leftward and down-rightward. Only the up-leftward portion is compatible with an increase of entropy across the shock; the down-rightward portion requires an entropy decrease, which is forbidden by the second law of thermodynamics, and therefore is not drawn on Fig. 17.11. The actual location (V_2, P_2) of the downstream state along the shock adiabat is determined by Eq. (17.31b) in a simple way: the slope of the dotted line connecting the upstream and downstream states is $-j^2$, where j is the mass flux passing through the shock. When one thereby has learned (V_2, P_2), one can compute the downstream speed v_2 from Eq. (17.31c).

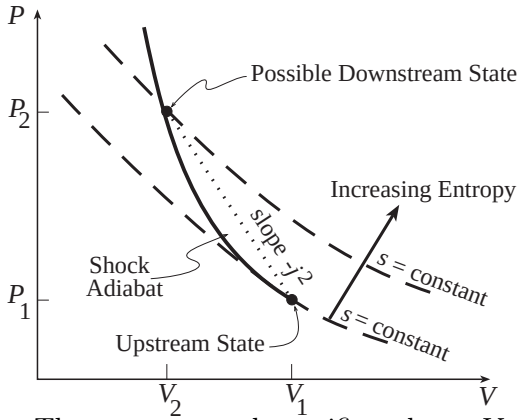

Fig. 17.11: Shock adiabat. The pressure and specific volume $V = 1/\rho$ in the upstream flow are P_1 and V_1, and in the downstream flow P_2 and V_2. The dashed curves are ordinary adiabats (curves of constant entropy per unit mass s). The thick curve is the *shock adiabat*, the curve of allowed downstream states (V_2, P_2) for a given upstream state (V_1, P_1). The actual location of the downstream state on this adiabat is determined by the mass flux j flowing through the shock: the slope of the dotted line connecting the upstream and downstream states is $-j^2$.

It can be shown that the pressure and density always increase across a shock (as is the case in Fig. 17.11), and the fluid always decelerates,

$$P_2 > P_1 \ , \quad V_2 < V_1 \ , \quad v_2 < v_1 \ ; \tag{17.33}$$

see Ex. 17.7. It also can be demonstrated in general, and will be verified in a particular case below, that the Rankine-Hugoniot relations require the flow to be supersonic with respect to the shock front upstream $v_1 > C_1$ and subsonic downstream, $v_2 < C_2$. Physically, this is sensible (as we have seen above): When the fluid approaches the shock supersonically, it is not possible to communicate a pressure pulse upstream from the shock (via a Riemann invariant moving at the speed of sound) and thereby cause the flow to decelerate; therefore, to slow the flow a shock must develop.[2] By contrast, the shock front can and does respond to changes in the downstream conditions, since it is in causal contact with the downstream flow; sound waves and a Riemann invariant can propagate upstream, through the downstream flow, to the shock.

To summarize, shocks are machines that decelerate a normally incident upstream flow to a subsonic speed, so it can be in causal contact with conditions downstream. In the process, bulk momentum flux, ρv^2, is converted into pressure, bulk kinetic energy is converted into internal energy, and entropy is manufactured by the dissipative processes at work in the shock front. For given upstream conditions, the downstream conditions are fixed by the conservation laws of mass, momentum and energy, and are independent of the detailed dissipation mechanisms.

****

EXERCISES

Exercise 17.7 *Derivation and Challenge: Signs of Change Across a Shock*

(a) Almost all equations of state satisfy the condition $(\partial^2 V/\partial P^2)_s > 0$. Show that, when this is satisfied, the Rankine-Hugoniot relations and the law of entropy increase imply that the pressure and density must increase across a shock and the fluid must decelerate; i.e., $P_2 > P_1$, $V_2 < V_1$, and $v_2 < v_1$.

(b) Show that in a fluid that violates $(\partial^2 V/\partial P^2)_s > 0$, the pressure and density must still increase and the fluid decelerate across a shock, as otherwise the shock would be unstable.

For a solution to this exercise, see Sec. 84 of Landau and Lifshitz (1959).

Exercise 17.8 ***T2*** *Problem: Relativistic Shock*
In astrophysics (e.g. in supernova explosions and in jets emerging from the vicinities of black holes), one sometimes encounters shock fronts for which the flow speeds relative to the shock approach the speed of light, and the internal energy density is comparable to the fluid's rest-mass density.

[2] Of course, if there is some faster means of communication, for example photons or, in an astrophysical context, cosmic rays or neutrinos, then there may be a causal contact between the shock and the inflowing gas, and this can either prevent shock formation or lead to a more complex shock structure.

(a) Show that the relativistic Rankine-Hugoniot equations for such a shock take the following form:

$$\boxed{\eta_2^2 - \eta_1^2 = (P_2 - P_1)(\eta_1 V_1 + \eta_2 V_2)}\,, \tag{17.34a}$$

$$\boxed{j^2 = \frac{P_2 - P_1}{\eta_1 V_1 - \eta_2 V_2}}\,, \tag{17.34b}$$

$$\boxed{v_2\gamma_2 = jV_2\ , \quad v_1\gamma_1 = jV_1}\,. \tag{17.34c}$$

Here, (i) we use units in which the speed of light is one (as in Chap. 2); (ii) $V \equiv 1/\rho_o$ is the volume per unit rest mass and ρ_o is the rest-mass density (equal to some standard rest mass per baryon times the number density of baryons; cf. Sec. 2.12.3); (iii) we denote the total density of mass-energy including rest mass by ρ_R (it was denoted ρ in Chap. 2) and the internal energy per unit rest mass by u so $\rho_R = \rho_o(1+u)$; and in terms of these the quantity $\eta \equiv (\rho_R + P)/\rho_o = 1 + u + P/\rho_o = 1 + h$ is the relativistic enthalpy per unit rest mass (i.e. the enthalpy per unit rest mass including the rest-mass contribution to the energy) as measured in the fluid rest frame; (iv) P is the pressure as measured in the fluid rest frame; (v) v is the flow velocity in the shock's rest frame and $\gamma \equiv 1/\sqrt{1-v^2}$ (*not* the adiabatic index!), so $v\gamma$ is the spatial part of the flow 4-velocity; and (vi) j is the rest-mass flux (rest mass per unit area per unit time) entering and leaving the shock.

(b) Use a pressure-volume diagram to discuss these relativistic Rankine-Hugoniot equations in a manner analogous to Fig. 17.11.

(c) Show that in the nonrelativistic limit, the relativistic Rankine-Hugoniot equations (17.34) reduce to the nonrelativistic ones (17.30).

(d) It can be shown (Thorne 1973) that, as for nonrelativistic shocks, so also relativistically, in general $P_2 > P_1$, $V_2 < V_1$ and $v_2 < v_1$. Consider, as an example, a relativistic shock propagating through a fluid in which the mass density due to radiation greatly exceeds that due to matter (a *radiation dominated fluid*), so $P = \rho_R/3$ (Sec. 3.5.5). Show that $v_1 v_2 = 1/3$, which implies $v_1 > 1/\sqrt{3}$ and $v_2 < 1/\sqrt{3}$. Show further that $P_2/P_1 = (v_1^2 - 1/3)\gamma_1^2$.

Exercise 17.9 ***Problem: Hydraulic Jumps and Breaking Ocean Waves*
Run water at a high flow rate from a kitchen tap onto a dinner plate (Fig. 17.12). What you see is called a hydraulic jump. It is the kitchen analog of a breaking ocean wave, and the shallow-water-wave analog of a shock front in a compressible gas. In this exercise you will develop the theory of hydraulic jumps (and breaking ocean waves) using the same tools as for shock fronts.

(a) Recall that for shallow-water waves, the water motion, below the water's surface, is nearly horizontal with speed independent of depth z (Ex. 16.1). The same is true of the water in front of and behind a hydraulic jump. Apply the conservation of mass and

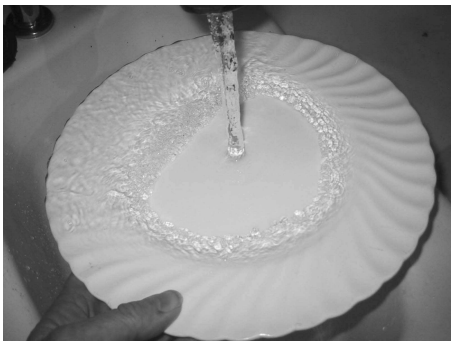

Fig. 17.12: Hydraulic jump on a dinner plate under a kitchen tap.

momentum to a hydraulic jump, in the jump's rest frame, to obtain equations for the height of the water h_2 and water speed v_2 behind the jump (emerging from it) in terms of those in front of the jump, h_1, v_1. These are the analog of the Rankine-Hugoniot relations for a shock front. [Hint: In momentum conservation you will need to use the pressure P as a function of height in front of and behind the jump.]

(b) You did not use energy conservation across the jump in your derivation, but it was needed in the analysis of a shock front. Why?

(c) Show that the upstream speed v_1 is greater than the speed $\sqrt{gh_1}$ of small-amplitude, upstream gravity waves [shallow-water waves; Eq. (16.10) and associated discussion]; i.e. the upstream flow is supersonic. Similarly show that the downstream flow speed v_2 is slower than the speed $\sqrt{gh_2}$ of small-amplitude, downstream gravity waves; i.e., the downstream flow is subsonic.

(d) We normally view a breaking ocean wave in the rest frame of the quiescent upstream water. Use your hydraulic-jump equations to show that the speed of the breaking wave as seen in this frame is related to the depths h_1 and h_2 in front of and behind the breaking wave by

$$v_{\rm break} = \left[\frac{g(h_1+h_2)h_2}{2h_1}\right]^{1/2} ;$$

see Fig. 17.13.

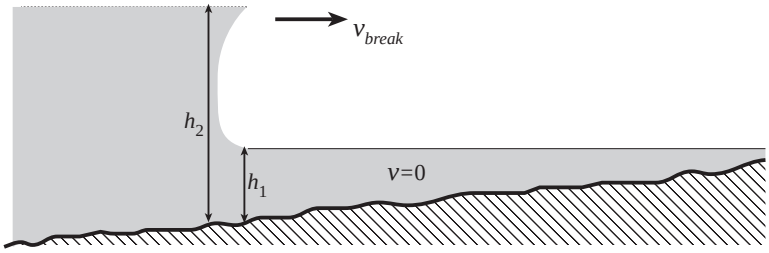

Fig. 17.13: Ocean wave breaking on a slowly sloping beach. The depth of water ahead of the wave is h_1 and the depth behind the wave is h_2.

****

17.5.2 Junction Conditions for Ideal Gas with Constant γ

To make the shock junction conditions more explicit, let us again specialize to an ideal gas with constant specific-heat ratio γ (a polytropic gas), so the equation of state is $u = PV/(\gamma-1)$ and the sound speed is $C = \sqrt{\gamma P/\rho} = \sqrt{\gamma PV}$ [Eqs. (17.2)]. We measure the strength of the shock using the *shock Mach number* M, which is defined to be the Mach number in the upstream flow relative to the shock,

$$M \equiv M_1 = v_1/C_1 = \sqrt{v_1^2/\gamma P_1 V_1}\ . \tag{17.35}$$

With the aid of this equation of state and Mach number, we can bring the Rankine-Hugoniot relations (17.31) into the form

$$\boxed{\frac{\rho_1}{\rho_2} = \frac{V_2}{V_1} = \frac{v_2}{v_1} = \frac{\gamma-1}{\gamma+1} + \frac{2}{(\gamma+1)M^2}}\ , \tag{17.36a}$$

$$\boxed{\frac{P_2}{P_1} = \frac{2\gamma M^2}{\gamma+1} - \frac{\gamma-1}{\gamma+1}}\ , \tag{17.36b}$$

$$\boxed{M_2^2 = \frac{2+(\gamma-1)M^2}{2\gamma M^2 - (\gamma-1)}}\ . \tag{17.36c}$$

Here $M_2 \equiv v_2/c_2$ is the downstream Mach number.

The results for this equation of state illustrate a number of general features of shocks: The density and pressure increase across the shock, the flow speed decreases, and the downstream flow is subsonic—all discussed above—and one important new feature: A shock weakens as its Mach number M decreases. In the limit that $M \to 1$, the jumps in pressure, density, and speed vanish and the shock disappears.

In the *strong-shock limit*, $M \gg 1$, the jumps are

$$\boxed{\frac{\rho_1}{\rho_2} = \frac{V_2}{V_1} = \frac{v_2}{v_1} \simeq \frac{\gamma-1}{\gamma+1}}\ , \tag{17.37a}$$

$$\boxed{\frac{P_2}{P_1} \simeq \frac{2\gamma M^2}{\gamma+1}}\ . \tag{17.37b}$$

Thus, the density jump is always of order unity, but the pressure jump grows ever larger as M increases. Air has $\gamma \simeq 1.4$ (Ex. 17.1), so the density compression ratio for a strong shock in air is $\rho_2/\rho_1 = 6$ and the pressure ratio is $P_2/P_1 = 1.2M^2$. The space shuttle's reentry provides a nice example of these strong-shock Rankine-Hugoniot relations; see bottom half of Box 17.4.

****

EXERCISES

Exercise 17.10 *Problem: Shock Tube*
Consider a shock tube as discussed in Sec. 17.4 and Fig. 17.11. Suppose that there is a small density of gas at rest in the evacuated half of the tube, with specific heat ratio γ_1 which might differ from that of the driver gas, and with initial sound speed C_1. After the membrane is ruptured, the driver gas will expand into the evacuated half of the tube forming a shock front. Show that, in the limit of very large pressure ratio across the shock, the shock Mach number is

$$M_1 \simeq \left(\frac{\gamma_1 + 1}{\gamma_1 - 1}\right)\left(\frac{C_0}{C_1}\right) \ ,$$

where C_0 is the driver gas's initial sound speed.

****

17.5.3 Internal Structure of a Shock

Although they are often regarded as discontinuities, shocks, like boundary layers, do have structure. The simplest case is that of a gas in which the shear viscosity coefficient is molecular in origin and is given by $\eta = \rho\nu \sim \rho\lambda v_{\rm th}/3$, where λ is the molecular mean free path and $v_{\rm th} \sim c$ is the mean thermal speed of the molecules (Ex. 3.19). In this case the viscous stress $T_{xx} = -\zeta\theta - 2\eta\sigma_{xx}$ is $-(\zeta + 4\eta/3)dv/dx$, where ζ is the coefficient of bulk viscosity which can be of the same order as the coefficient of shear viscosity. In the shock, this must roughly balance the total kinetic momentum flux $\sim \rho v^2$. If we estimate the velocity gradient dv/dx by v_1/δ_S where δ_S is a measure of the shock thickness and we estimate the sound speed in the shock front by $C \sim v_1$, then we deduce that the shock thickness δ_S is roughly equal to λ, the collision mean free path in the gas. For air at standard temperature and pressure, the mean free path is $\lambda \sim (\sqrt{2}n\pi\sigma^2)^{-1} \sim 70$ nm, where n is the molecular density and σ is the molecular diameter. This is very small! Microscopically, it makes sense that $\delta_S \sim \lambda$ as an individual molecule only needs a few collisions to randomize its ordered motion perpendicular to the shock front. However, this estimate raises a problem as it brings into question our use of the continuum approximation (cf. Sec. 13.1). It turns out that, when a more careful calculation of the shock structure is carried out incorporating heat conduction, the shock thickness is several mean free paths, fluid dynamics is acceptable for an approximate theory, and the results are in rough accord with measurements of the velocity profiles of shocks with modest Mach numbers. Despite this, for an accurate description of the shock structure, a kinetic treatment is usually necessary.

So far we have assumed that the shocked fluid is made of uncharged molecules. A more complicated type of shock can arise in an ionized gas, i.e. a plasma (Part V). Shocks in the solar wind are examples. In this case, the collision mean free paths are enormous, in fact comparable with the transverse size of the shock, and therefore one might expect the shocks to be so thick that the Rankine-Hugoniot relations will fail. However, spacecraft measurements reveal solar-wind shocks that are relatively thin—far thinner than the collisional mean free paths of the plasma's electrons and ions. In this case, it turns out that collisionless, collective elctromagnetic & charged-particle interactions in the plasma are responsible for the viscosity

and dissipation. (The particles create plasma waves, which in turn deflect the particles.) These processes are so efficient that thin shock fronts can occur without individual particles having to hit one another. Since the shocks are thin, they must satisfy the Rankine-Hugoniot relations. We shall discuss these collisionless shocks further in Sec. 23.6.

17.5.4 Mach Cone

The shock waves formed by a supersonically moving body are quite complex close to the body and depend on its detailed shape, Reynolds' number, etc.; see, e.g., Fig. 17.1 above. However, far from the body, the leading shock has the form of the *Mach cone* shown in Fig. 17.14. We can understand this cone by the construction shown in the figure. The shock is the boundary between that fluid which is in sound-based causal contact with the projectile and that which is not. This boundary is mapped out by (conceptual) sound waves that propagate into the fluid from the projectile at the ambient sound speed C_0. When the projectile is at the indicated position, the envelope of the circles is the shock front and has the shape of the Mach cone, with opening angle (the *Mach angle*)

$$\boxed{\alpha = \sin^{-1}(1/M)} \,. \tag{17.38}$$

Usually, there will be two such shock cones, one attached to the projectile's bow shock and the other formed out of the complex shock structure in its tail region. The pressure must jump twice, once across each of these shocks, and will therefore form an *N wave* which propagates cylindrically away from the projectile as shown in Fig. 17.15. Behind the first shock, the density and pressure drop off gradually by more than the first shock's compression. As a result, the fluid flowing into the second shock has a lower pressure, density, and sound speed than that flowing into the first (cf. Fig. 17.15). This causes the Mach number of the second shock to be higher than that of the first, and its Mach angle thus to be smaller. As a result, the separation between the shocks increases as they travel, $\propto \varpi^{1/2}$ it turns out; and the pressure jumps across the shocks decrease $\propto \varpi^{-3/4}$. Here ϖ is the perpendicular distance of the point of observation from the projectile's trajectory. Often a double boom can be heard on the ground. For a detailed analysis see Sec. 9.3 of Whitham (1974).

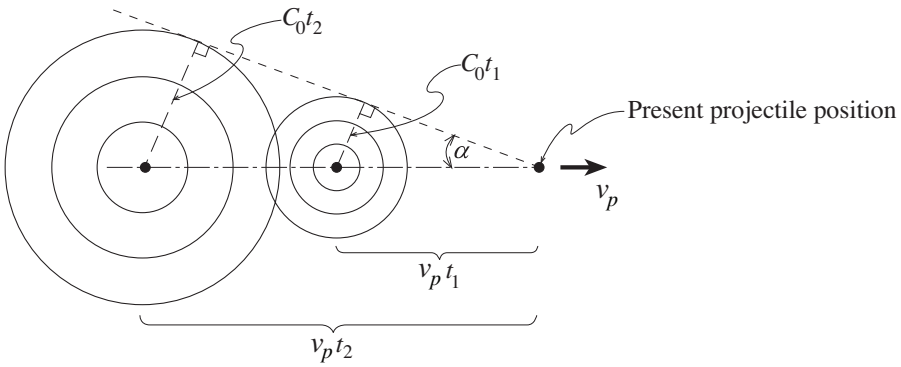

Fig. 17.14: Construction for Mach cone formed by a supersonic projectile. The cone angle is $\alpha = \sin^{-1}(M^{-1})$, where $M = v_p/C_0$ is the Mach number of the projectile.

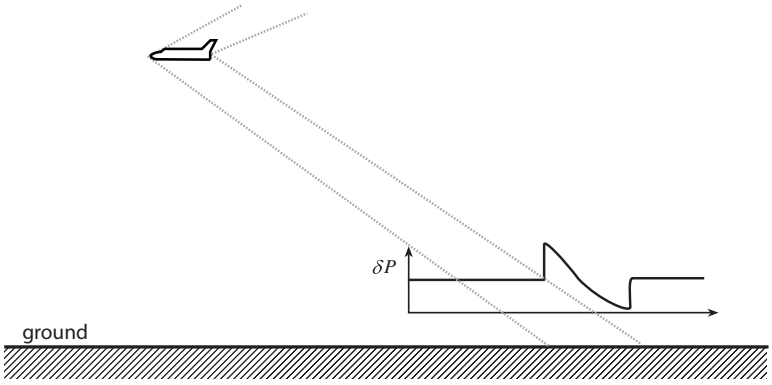

Fig. 17.15: Double shock created by supersonic body and associated "N wave" pressure distribution on the ground.

****

EXERCISES

Exercise 17.11 *Problem: Sonic Boom from the Space Shuttle*
Use the quoted scaling of N wave amplitude with cylindrical radius ϖ to make an order of magnitude estimate of the flux of acoustic energy produced by the space shuttle flying at Mach 2 at an altitude of 20km. Quote your answer in dB [cf. Eq. (16.61)].

****

17.6 Self-Similar Solutions — Sedov-Taylor Blast Wave

Strong explosions can generate shock waves. Examples include atmospheric nuclear explosions, supernova explosions, and depth charges. The debris from a strong explosion will be at much higher pressure than the surrounding gas and will therefore drive a strong spherical shock into the surroundings. Initially, this shock wave will travel at roughly the radial speed of the expanding debris. However, the mass of fluid swept up by the shock will eventually exceed that of the explosion debris. The shock will then decelerate and the energy of the explosion will be transferred to the swept-up fluid. It is of obvious importance to be able to calculate how fast and how far the shock front will travel.

17.6.1 The Sedov-Taylor Solution

We first make an order of magnitude estimate. Let the total energy of the explosion be E and the density of the surrounding fluid (assumed uniform) be ρ_0. Then after time t, when the shock radius is $R(t)$, the mass of swept-up fluid will be $m \sim \rho_0 R^3$. The fluid velocity behind the shock will be roughly the radial velocity of the shock front, $v \sim \dot{R} \sim R/t$, and so the kinetic energy of the swept-up gas will be $\sim mv^2 \sim \rho_0 R^5/t^2$. There will also be internal energy in the post-shock flow, with energy density roughly equal to the post-shock

pressure, $\rho u \sim P \sim \rho_0 \dot{R}^2$ [cf. the strong-shock jump condition (17.36b) with $P_1 \sim \rho_0 C_0^2$ so $P_1 M^2 \sim \rho_0 v^2 \sim \rho_0 \dot{R}^2$]. The total internal energy within the expanding shock will then be $\sim \rho \dot{R}^2 R^3 \sim \rho_0 R^5/t^2$, equal in order of magnitude to the kinetic energy. Equating this to the total energy E of the explosion, we obtain the estimate

$$E = \kappa \rho_0 R^5 t^{-2} \,, \tag{17.39}$$

where κ is a numerical constant of order unity. This implies that at time t the shock front has reached the radius

$$R = \left(\frac{E}{\kappa \rho_0}\right)^{1/5} t^{2/5} \,. \tag{17.40}$$

This scaling should hold roughly from the time that the mass of the swept-up gas is of order that of the exploding debris, to the time that the shock weakens to a Mach number of order unity so we can no longer use the strong-shock value $\sim \rho_0 \dot{R}^2$ for the post-shock pressure.

Note that we could have obtained Eq. (17.40) by a purely dimensional argument: E and ρ_0 are the only significant controlling parameters in the problem, and $E^{1/5}\rho_0^{-1/5}t^{2/5}$ *is the only quantity with dimensions of length that can be constructed from* E, ρ_0 *and* t. However, it is usually possible and always desirable to justify any such dimensional argument on the basis of the governing equations.

If, as we shall assume, the motion remains radial and the gas is ideal with constant specific-heat ratio γ, then we can solve for the details of the flow behind the shock front by integrating the radial flow equations

$$\frac{\partial \rho}{\partial t} + \frac{1}{r^2}\frac{\partial}{\partial r}(r^2 \rho v) = 0 \,, \tag{17.41a}$$

$$\frac{\partial v}{\partial t} + v\frac{\partial v}{\partial r} + \frac{1}{\rho}\frac{\partial P}{\partial r} = 0 \,, \tag{17.41b}$$

$$\frac{\partial}{\partial t}\left(\frac{P}{\rho^\gamma}\right) + v\frac{\partial}{\partial r}\left(\frac{P}{\rho^\gamma}\right) = 0 \,. \tag{17.41c}$$

The first two equations are the familiar continuity equation and Euler equation written for a spherical flow. The third equation is energy conservation expressed as the adiabatic-expansion relation, P/ρ^γ =constant moving with a fluid element. Although P/ρ^γ is time-independent for each fluid element, its value will change from element to element. Gas that has passed through the shock more recently will be given a smaller entropy than gas which was swept up when the shock was stronger, and thus will have a smaller value of P/ρ^γ.

Given suitable initial conditions, the partial differential equations (17.41) can be integrated numerically. However, there is a practical problem: it is not easy to determine the initial conditions in an explosion! Fortunately, at late times, when the inital debris mass is far less than the swept-up mass, the fluid evolution is independent of the details of the initial expansion and in fact can be understood analytically as a *similarity solution*. By this, we mean that the shape of the radial profiles of pressure, density and velocity are independent of time.

We have already met three examples of similarity solutions: the Blasius structure of a laminar boundary layer (Sec. 14.4.1), the structure of a turbulent jet (Ex. 15.3), and the flow

of water following the sudden rupture of a dam (Ex. 16.9). The one we explored in greatest detail was the Blasius boundary layer (Sec. 14.4.1). There we argued on the basis of mass and momentum conservation (or, equally well, via dimensional analysis) that the thickness of the boundary layer as a function of distance x downstream would be $\sim \delta = (\nu x/V)^{1/2}$ where V was the speed of the flow above the boundary layer. This motivated us to introduce the dimensionless variable $\xi = y/\delta$ and argue that the boundary layer's speed $v_x(x, y)$ would be equal to the free stream velocity V times some universal function $f'(\xi)$. This ansatz converted the fluid's partial differential equations into an ordinary differential equation for $f(\xi)$, which we solved numerically.

Our explosion problem is somewhat similar. The characteristic scaling length in the explosion is the radius $R(t) = (E/\kappa\rho_0)^{1/5}t^{2/5}$ of the shock [Eq. (17.40)], with κ an as-yet-unknown constant, so the fluid and thermodynamic variables should be expressible as some characteristic values multiplying universal functions of

$$\xi \equiv r/R(t) \ . \tag{17.42}$$

Our thermodynamic variables are P, ρ, u, and natural choices for their characteristic values are the values P_2, ρ_2, v_2 immediately behind the shock. If we assume the shock is strong, then we can use the strong-shock jump conditions (17.37) to determine those values, and then write

$$P = \frac{2}{\gamma+1}\rho_0\dot{R}^2\tilde{P}(\xi) \ , \tag{17.43a}$$

$$\rho = \frac{\gamma+1}{\gamma-1}\rho_0 \ \tilde{\rho}(\xi) \ , \tag{17.43b}$$

$$v = \frac{2}{\gamma+1}\dot{R} \ \tilde{v}(\xi) \ , \tag{17.43c}$$

with $\tilde{P}(1) = \tilde{\rho}(1) = \tilde{v}(1) = 1$ since $\xi = 1$ is the shock's location. Note that the velocity v is scaled to the post-shock velocity v_2 measured in the inertial frame in which the upstream fluid is at rest, rather than in the non-inertial frame in which the decelerating shock is at rest. The self-similarity ansatz (17.43) and resulting similarity solution for the flow are called the *Sedov-Taylor blast-wave solution*, since L. I. Sedov and G. I. Taylor independently developed it.

The partial differential equations (17.41) can now be transformed into ordinary differential equations by inserting the ansatz (17.43) together with expression (17.40) for $R(t)$, changing the independent variables from r, t to R, ξ, and using

$$\left(\frac{\partial}{\partial t}\right)_r = -\left(\frac{\xi\dot{R}}{R}\right)\left(\frac{\partial}{\partial\xi}\right)_R + \dot{R}\left(\frac{\partial}{\partial R}\right)_\xi = -\left(\frac{2\xi}{5t}\right)\left(\frac{\partial}{\partial\xi}\right)_R + \frac{2R}{5t}\left(\frac{\partial}{\partial R}\right)_\xi \ , \tag{17.44}$$

$$\left(\frac{\partial}{\partial r}\right)_t = \left(\frac{1}{R}\right)\left(\frac{\partial}{\partial\xi}\right)_R \ . \tag{17.45}$$

Mass conservation, the Euler equation, and the equation of adiabatic expansion become, in

that order:

$$0 = 2\tilde{\rho}\tilde{v}' - (\gamma+1)\xi\tilde{\rho}' + \tilde{v}\left(2\tilde{\rho}' + \frac{4}{\xi}\tilde{\rho}\right) , \tag{17.46a}$$

$$0 = \tilde{\rho}\tilde{v}[3(\gamma+1) - 4\tilde{v}'] + 2(\gamma+1)\xi\tilde{\rho}\tilde{v}' - 2(\gamma-1)\tilde{P}' , \tag{17.46b}$$

$$3 = \left(\frac{2\tilde{v}}{\gamma+1} - \xi\right)\left(\frac{\tilde{P}'}{\tilde{P}} - \gamma\frac{\tilde{\rho}'}{\tilde{\rho}}\right) . \tag{17.46c}$$

These self-similarity equations can be solved numerically, subject to the boundary conditions that $\tilde{v}$, $\tilde{\rho}$ and $\tilde{P}$ are all zero at $\xi = 0$ and 1 at $\xi = 1$. Remarkably, Sedov (1957) found an analytic solution, which is given in Sec. 99 of Landau and Lifshitz (1959) and in Sedov (1993). The solution for an explosion in air ($\gamma = 1.4$) are exhibited in Fig. 17.16.

Armed with the solution for $\tilde{v}(\xi), \tilde{\rho}(\xi), \tilde{P}(\xi)$ (numerical or analytic), we can evaluate the flow's energy E, which is equal to the explosion's total energy during the time interval when this similarity solution is accurate. The energy E is given by the integral

$$\begin{aligned} E &= \int_0^R 4\pi r^2 dr\rho\left(\frac{1}{2}v^2 + u\right) \\ &= \frac{4\pi\rho_0 R^3\dot{R}^2(\gamma+1)}{(\gamma-1)}\int_0^1 d\xi\xi^2\tilde{\rho}\left(\frac{2\tilde{v}^2}{(\gamma+1)^2} + \frac{2\tilde{P}}{(\gamma+1)^2\tilde{\rho}}\right) . \end{aligned} \tag{17.47}$$

Here we have used Eqs. (17.43) and substituted $u = P/\rho(\gamma-1)$ for the internal energy [Eq. (17.2b)]. The energy E appears not only on the left side of this equation, but also on the right, in the terms $\rho_o R^3\dot{R}^2 = (4/25)E/\kappa$. Thus, E cancels out, and Eq. (17.47) becomes an equation for the unknown constant κ. Evaluating that equation numerically, we find that κ varies from $\kappa = 0.86$ for $\gamma = 1.4$ (air) to $\kappa = 0.49$ for $\gamma = 1.67$ (monatomic gas or fully ionized plasma).

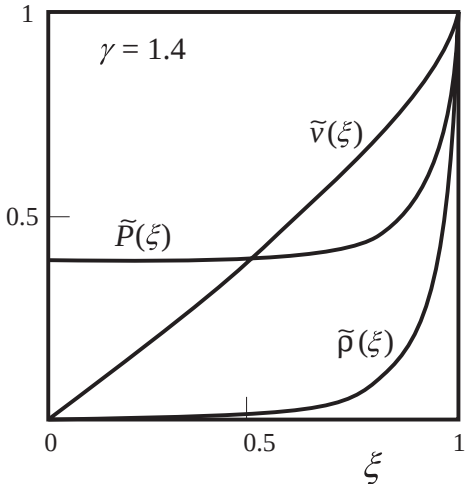

Fig. 17.16: Scaled pressure, density and velocity as a function of scaled radius behind a Sedov-Taylor blast wave in air with $\gamma = 1.4$.

It is enlightening to see how the fluid behaves in this blast-wave solution. The fluid that passes through the shock is compressed so that it mostly occupies a fairly thin spherical shell immediately behind the shock [see the spike in $\tilde{\rho}(\xi)$ in Fig. 17.16]. The fluid in this shell moves somewhat more slowly than the shock [$v = 2\dot{R}/(\gamma+1)$; Eq. (17.43c) and Fig. 17.16]; i.e., it flows from the shock front through the high-density shell (fairly slowly relative to the shell which remains attached to the shock), and on into the lower density post-shock region. Since the post-shock flow is subsonic, the pressure within the blast wave is fairly uniform [see the curve $\tilde{P}(\xi)$ in fig. 17.16]; in fact the central pressure is typically about half the maximum pressure immediately behind the shock. This pressure pushes on the spherical shell, thereby accelerating the freshly swept-up fluid.

17.6.2 Atomic Bomb

The first atomic bomb was exploded in New Mexico in 1945, and photographs released in 1947 (Fig. 17.17) showed the radius of the blast wave as a function of time. The pictures were well fit by $R \sim 37(t/1\text{ms})^{0.4}$ up to about $t = 100$ ms when the shock Mach number fell to about unity (Fig. 17.17). Combining this information with the the above similarity solution, which they had earlier derived independently (Taylor 1941, Sedov 1946), the Russian physicist L. I. Sedov and the British physicist G. I. Taylor were both able to infer the total energy released, which was an official American secret at the time. Their analyses of the data were published later: Taylor (1950), Sedov (1957, 1993).

Adopting the specific heat ratio $\gamma = 1.4$ of air, the corresponding value $\kappa = 0.86$, and the measured $R \sim 37(t/1\text{ms})^{0.4}$, we obtain from Eq. (17.47) the estimate $E \sim 7.2 \times 10^{13}$ j, which is about the same energy release as 17 kilotons of TNT. This estimate is close to the Los Alamos scientists estimate of 18 to 20 kilotons. (Hydrogen bombs have been manufactured over a thousand times more energetic than this—as much as 57 megatons—but such awesome weapons have not been deemed militarily useful, so today's arsenals contain bombs that are typically *only* ∼one megaton!)

We can use the Sedov-Taylor solution to infer some further features of the explosion. The post-shock gas is at density $\sim (\gamma+1)/(\gamma-1) \sim 5$ times the ambient density $\rho_0 \sim 1$ kg m^{-3}. Similarly, using the ideal gas law $P = (\rho/m_p\mu)k_BT$ with a mean molecular weight $\mu \sim 10$ and the strong-shock jump conditions (17.37), the post-shock temperature can be computed:

$$T_2 = \frac{m_p\mu}{\rho_2 k_B} P_2 \sim 4 \times 10^4 \left(\frac{t}{1\text{ms}}\right)^{-1.2} \text{K} \; . \tag{17.48}$$

At early times, this is high enough to ionize the gas.

17.6.3 Supernovae

The evolution of most massive stars ends in a supernova explosion (like that which was observed in 1987 in the Large Magellanic Cloud), in which a neutron star of mass $m \sim 3\times10^{30}$ kg is formed. This neutron star has a gravitational binding energy of about $0.1mc^2 \sim 3\times10^{46}$ J. Most of this binding energy is released in the form of neutrinos in the collapse that forms the neutron star, but an energy $E \sim 10^{44}$J drives off the outer envelope of the pre-supernova

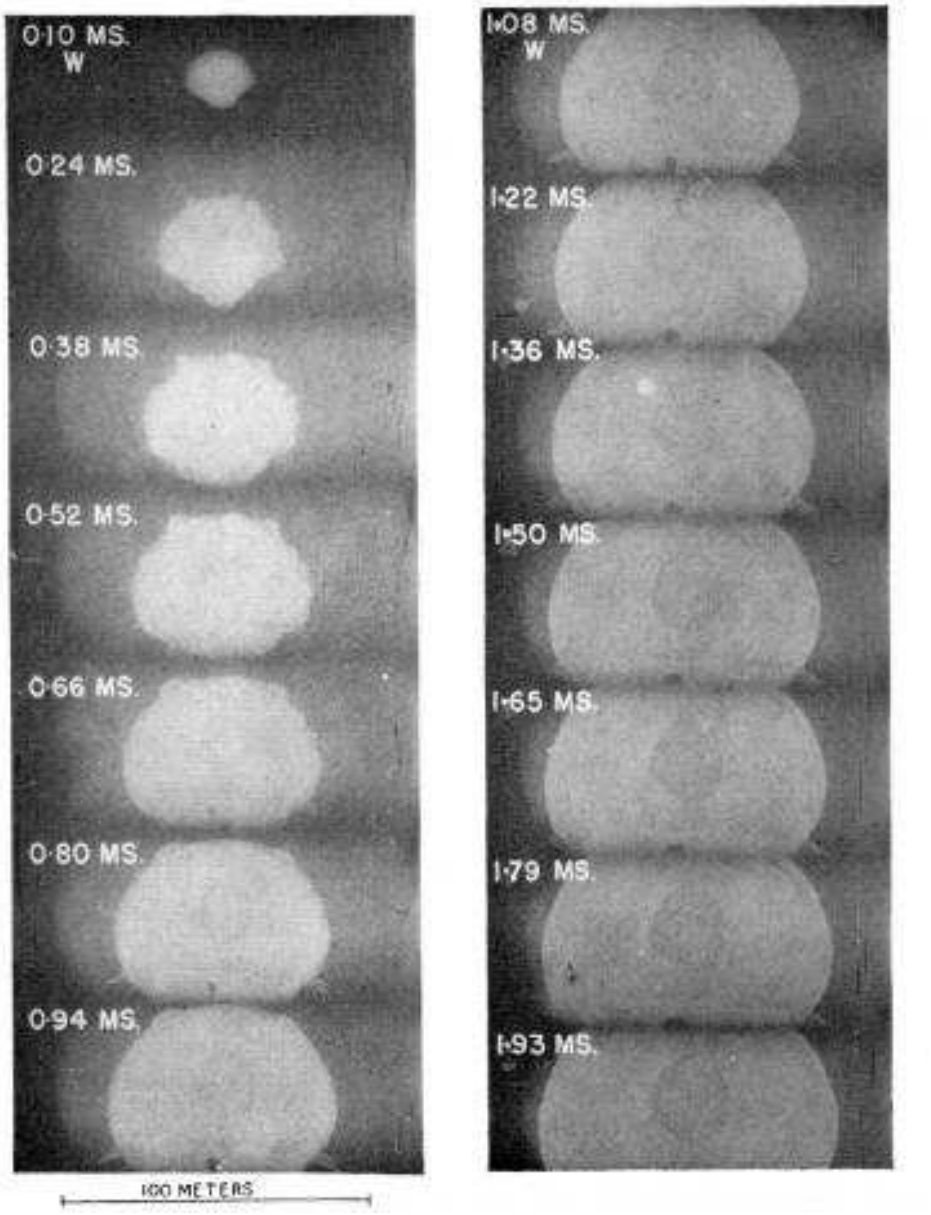

Fig. 17.17: Photoraphs of the fireball (very hot post-shock gas) from the first atomic bomb explosion, at Almagordo New Mexico on 16 July 1945; from Mack (1947).

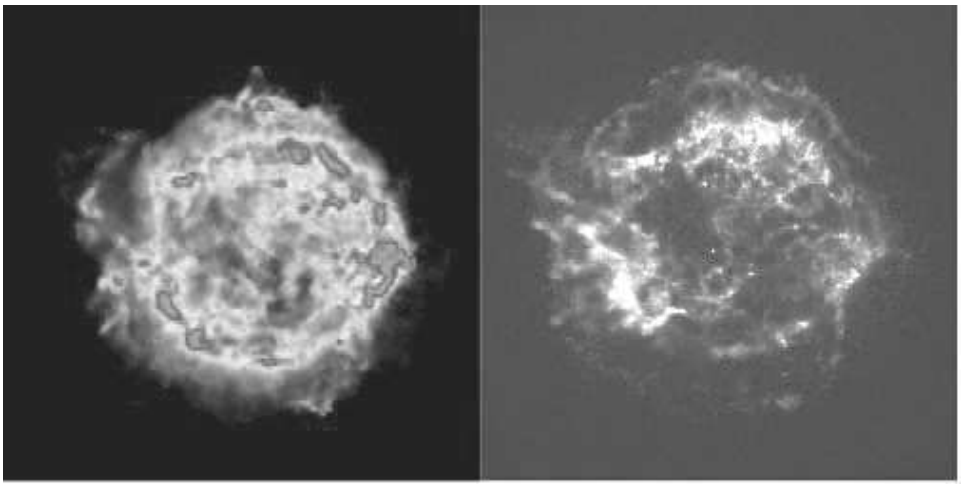

Fig. 17.18: Cassiopeia A – a supernova remnant left behind by an exploding star in our Milky Way galaxy approximately 300 years ago. The image to the left was made using the Very Large Array Radio Telescope; that to the right by the Chandra X-ray Observatory.

star, a mass $M_0 \sim 10^{31}$kg. This stellar material escapes with a rms speed $V_0 \sim (2E/M_0)^{1/2} \sim$ 5000 km s^{-1}. The expanding debris drives a blast wave into the surrounding interstellar medium, which has density $\rho_0 \sim 10^{-21}$kg m^{-3}. The expansion of the blast wave can be modeled using the Sedov-Taylor solution after the swept-up interstellar gas has become large enough to dominate the blast debris, so the star-dominated initial conditions are no longer important—i.e. after a time $\sim (3M_0/4\pi\rho_0)^{1/3}/V_0 \sim 1000$ yr. The blast wave then decelerates in a Sedov-Taylor similarity way until the shock speed nears the sound speed in the surrounding gas; this takes about $100,000$ yr. *Supernova remnants* of this sort are efficient emitters of radio waves, and several hundred have been observed in our Milky Way galaxy.

In some of the younger examples, like Cassiopeia A (Fig. 17.18), it is possible to determine the expansion speed, and the effects of deceleration can be measured. The observations are consistent with the prediction of the Sedov-Taylor solution, namely that the radius varies as $R \propto t^{2/5}$, or $\ddot{R} = -3\dot{R}^2/2R$.

****

EXERCISES

Exercise 17.12 *Problem: Underwater explosions*
A simple analytical solution to the Sedov-Taylor similarity equations, can be found for the particular case $\gamma = 7$. This is a fair approximation to the behavior of water under explosive conditions, as it will be almost incompressible.

(a) Make the *ansatz* (whose self-consistency we will check later), that the velocity in the post-shock flow varies linearly with radius from the origin to the shock, i.e. $\tilde{v}(\xi) = \xi$. Use Eq. (17.44) to transform the equation of continuity into an ordinary differential equation and hence solve for the density function $\tilde{\rho}(\xi)$.

(b) Next use the equation of motion to discover that $\tilde{P}(\xi) = \xi^3$.

(c) Verify that your solutions for the functions $\tilde{P}, \tilde{\rho}, \tilde{v}$ satisfy the remaining entropy equation thereby vindicating the original *ansatz*.

(d) Finally, substitute into Eq. (17.47) to show that

$$E = \frac{2\pi R^5 \rho_0}{225 t^2}$$

(e) An explosive charge weighing 100kg with an energy release of 10^8J kg^{-1} is detonated underwater. For what range of shock radii do you expect that the Sedov-Taylor similarity solution will be valid?

Exercise 17.13 *Problem: Stellar Winds*
Many stars possess powerful stellar winds which drive strong spherical shock waves into the surrounding interstellar medium. If the strength of the wind remains constant, the kinetic and internal energy of the swept-up interstellar medium will increase linearly with time.

(a) Modify the text's analysis of a point explosion to show that in this case the speed of the shock wave at time t is $3R(t)/5t$, where R is the associated shock radius. What is the speed of the post-shock gas?

(b) Now suppose that the star explodes as a supernova and the blast wave expands into the relatively slowly moving stellar wind. Suppose that before the explosion the rate at which mass left the star and the speed of the wind were constant for a long time. How do you expect the density of gas in the wind to vary with radius? Modify the Sedov-Taylor analysis again to show that the expected speed of the shock wave at time t is now $2R(t)/3t$.

Exercise 17.14 *Problem: Similarity Solution for Shock Tube*
Use a similarity analysis to derive the solution (17.27) for the shock-tube flow depicted in Fig. 17.9.

****

Bibliographic Note

For physical insight into compressible flows and shock waves, we recommend the movies cited in Box 17.2. For textbook treatments, we recommend Anderson (2003), Liepmann and Roshko (1968), Thompson (1984), the relevant sections of Landau and Lifshitz (1959); and, at a more elementary and sometimes cursory level, Lautrup (2005). Whitham (1974) is superb on all aspects, from an applied mathematician's viewpoint.

Box 17.5
Important Concepts in Chapter 17

- γ-law equation of state, $P = K(s)\rho^\gamma$, Sec. 17.2
  - Values of γ for various situations, Sec. 17.2, Ex. 17.1
- Mach number, subsonic flow, supersonic flow, Sec. 17.3.1
- Quasi-one-dimensional transonic flow, Sec. 17.3
  - Opposite signs of dv/dA in supersonic vs. subsonic flow; and of $d\rho/dA$, Sec. 17.3.1
  - Sonic point and critical point of flow, Secs. 17.3.1 and 17.3.2
  - How a rocket engine works, and its De Laval nozzle, Sec. 17.3.3
- Transonic accretion of gas onto a neutron star or black hole, Ex. 17.4
- Riemann invariants for one-dimensional, time-dependent compressible flow, Sec. 17.4.1
  - Their use to compute the details of the flow, Secs. 17.4.1, 17.4.2
- Steepening of a nonlinear sound wave to form a shock, Sec. 17.4.1, Fig. 17.8
- Shock tube, Sec. 17.4.2
- Shock waves, Sec. 17.5
  - Upstream and downstream sides of the shock, Sec. 17.5
  - Adiabatic shock, Sec. 17.5.1
  - Continuity of normal fluxes of mass, momentum and energy across an adiabatic shock, Sec. 17.5.1
  - Rankine-Hugoniot relations for shock; shock adiabat, Secs. 17.5.1, and 17.5.2; and Ex. 17.8 in relativistic regime
  - Internal structure and thickness of a shock and role of viscosity, Sec. 17.5.3
  - Mach cone, N-wave and sonic boom, Sec. 17.5.4 and Ex. 17.11
  - Hydraulic jump and breaking ocean waves, Ex. 17.9
- Sedov-Taylor similarity solution for the flow behind a shock, Sec. 17.6
  - Application to bombs and supernovae, Secs. 17.6.2, 17.6.3

Engineering-oriented textbooks on fluid mechanics generally contain detailed treatments of quasi-one-dimensional flows, shocks, hydraulic jumps, and their real-world applications. We like White (2008); Munson, Young and Okiishi (2006); and Potter et. al. (2012).

The two-volume treatise by Zel'dovich and Raizer (1979) is a compendium of insights into shock waves and high-temperature hydrodynamics by an author (Yakov Borisovich Zel'dovich) who had a huge influence in the design of nuclear and thermonuclear weapons in the USSR and later on astrophysics and cosmology. Sedov (1993) — the tenth edition of a book whose first was in 1943 — is a classic and insightful treatise on similarity methods in physics.

Bibliography

Anderson, John D. 2003. *Modern Compressible Flow: With Historical Perspective*, New York: McGraw-Hill.

Bondi, H. 1952. *Monthly Notices of the Royal Astronomical Society*, **112**, 195.

Bryson, A. E. 196? *Waves in Fluids* a movie (National Committee for Fluid Mechanics Films); available in 2012 at `http://web.mit.edu/hml/ncfmf.html` .

Coles, D. 1965. *Channel Flow of a Compressible Fluid*, a movie (National Committee for Fluid Mechanics Films); available at `http://web.mit.edu/fluids/www/Shapiro/ncfmf.html` .

Landau, L. D. and Lifshitz, E. M. 1959. *Fluid Mechanics*, Reading, Massachusetts: Addison Wesley.

Liepmann, H. & Roshko, A. 1968. *Compressible Gas Dynamics*.

Mack, J. E. 1947. *Semi-popular Motion Picture Record of the Trinity Explosion*, MDDC221. U.S. Atomic Energy Commission.

Munson, Bruce R., Young, Donald F., and Okiishi, Theodore H. 2006. *Fundamentals of Fluid Mechanics*, Fifth Edition, New York: Wiley

Potter, Merle C., Wiggert, David C., Ramadan, Bassem H. 2012. *Mechanics of Fluids*, Fourth Edition, Stamford CT: Cengage Learning.

Rouse, H. 196?. *Effects of Fluid Compressibility*, a movie, available in 2002 at `http://www.iihr.uiowa.edu/research/publications-and-media/films-by-hunter-rouse/` .

Sedov, L. I. 1946. "Propagation of Strong Blast Waves", *Prikhlandnaya Matematika i Mekhanika*, **10**, 241–250.

Sedov, L. I. 1957, Russian language fourth edition of Sedov (1993).

Sedov, L. I. 1993. *Similarity and Dimensional Methods in Mechanics*, tenth edition, Boca Raton, Florida: CRC Press.

Thompson, P. A. 1984. *Compressible Fluid Dynamics*, Maple Press Co.

Thorne, Kip S. 1973. "Relativistic shocks: The Taub Adiabat", *Astrophysical Journal* **179**, 897–907.

Van Dyke, M. 1982. *An Album of Fluid Flow*, Stanford: Parabolic Press.

Whitham, G. B. 1974. *Linear and Nonlinear Waves*, New York: Wiley.

White, Frank M. 2008. *Fluid Mechanics*, New York: McGraw-Hill.

Zel'dovich, Ya. B. & Raizer, Yu. P. 1979. *Physics of Shock Waves and High Temperature Hydrodynamic Phenomena*.